1 **Increased pyroptosis activation in white matter microglia is associated**

2 **with neuronal loss in ALS motor cortex**

3 Evelien Van Schoor (1,2,3), Simona Ospitalieri (1), Sebastiaan Moonen (1, 3, 4), Sandra O. Tomé (1),

4 Alicja Ronisz (1), Orkun Ok (1), Jochen Weishaupt (5,6), Albert C. Ludolph (5,7), Philip Van Damme

5 (2,3,8), Ludo Van Den Bosch (2,3), Dietmar Rudolf Thal (1,9)

6 **Affiliations**

7 1. Laboratory of Neuropathology, Department of Imaging and Pathology, KU Leuven

8 (University of Leuven), Leuven Brain Institute (LBI), Leuven, Belgium.

9 2. Laboratory of Neurobiology, Department of Neurosciences, KU Leuven (University of

10 Leuven), Leuven Brain Institute (LBI), Leuven, Belgium.

11 3. Center for Brain & Disease Research, VIB, Leuven, Belgium.

12 4. Laboratory for the Research of Neurodegenerative Diseases, Department of Neurosciences,

13 KU Leuven (University of Leuven), Leuven Brain Institute (LBI), Leuven, Belgium

14 5. Department of Neurology, Ulm University, Ulm, Germany.

15 6. Divisions of Neurodegeneration, Department of Neurology, Mannheim Center for

16 Translational Neurosciences, Medical Faculty Mannheim, Heidelberg University, Mannheim,

17 Germany.

18 7. Deutsches Zentrum für Neurodegenerative Erkrankungen, Ulm, Germany.

19 8. Department of Neurology, University Hospitals Leuven, Leuven, Belgium.

20 9. Department of Pathology, University Hospitals Leuven, Leuven, Belgium.

21

22 **Corresponding author**

23 Dietmar R. Thal

24 Laboratory for Neuropathology

25 O&N IV Herestraat 49 - bus 1032

26 3000 Leuven

27 Tel.: 0032/16/3-44047

28 E-mail address: dietmar.thal@kuleuven.be

29

30 Evelien Van Schoor

31 Laboratory for Neuropathology

32 O&N IV Herestraat 49 – bus 1032

33 3000 Leuven

34 Tel.: 0032/16/3-44047

35 E-mail address: evelien.vanschoor@kuleuven.be

36

37 *Number of figures (main): 7*

38 *Number of tables (main): 4*

39 *Number of figures (supplementary): 10*

40 *Number of tables (supplementary): 6*

41

42

54 **Ethical Approval**

55 Human brain and spinal cord tissues were collected in accordance with the applicable laws in

56 Belgium (UZ Leuven) and Germany (Ulm). The recruitment protocols for collecting the human

57 brains were approved by the ethical committees of the University of Ulm (Germany) and of UZ

58 Leuven (Belgium). This study was approved by the UZ Leuven ethical committee (Leuven,

59 Belgium). All animal care and experiments were approved by the KU Leuven Ethical

60 Committee and were carried out according to the Belgian law.

61 **Availability of data and material**

62 Most data generated or analyzed during this study are included in this published manuscript and

63 in its supplementary information files. Additional data are available from the corresponding

64 author upon reasonable request.

65

66   **Keywords**

67   Amyotrophic lateral sclerosis, inflammasome, pyroptosis, transactive response DNA-binding

68   protein

69   **Abstract**

70   Amyotrophic lateral sclerosis (ALS) is characterized by the degeneration of motor neurons in

71   the motor cortex, brainstem and spinal cord. Although ALS is considered a motor neuron

72   disorder, neuroinflammation also plays an important role. Recent evidence in ALS disease

73   models indicates activation of the inflammasome and subsequent initiation of pyroptosis, an

74   inflammatory type of cell death. In this study, we determined the expression and distribution of

75   the inflammasome and pyroptosis effector proteins in *post-mortem* brain and spinal cord from

76   ALS patients (n = 25) and controls (n = 19), as well as in symptomatic and asymptomatic TDP-

77   43^{A315T} transgenic and wild-type mice. Further, we evaluated its correlation with the presence

78   of TDP-43 pathological proteins and neuronal loss. Expression of the NOD-, LRR- and pyrin

79   domain-containing protein 3 (NLRP3) inflammasome, pyroptosis effector protein cleaved

80   Gasdermin D (GSDMD), and IL-18 was detected in microglia in human ALS motor cortex and

81   spinal cord, indicative of canonical inflammasome-triggered pyroptosis activation. The number

82   of cleaved GSDMD-positive precentral white matter microglia was increased compared to

83   controls and correlated with a decreased neuronal density in human ALS motor cortex. Neither

84   of this was observed in the spinal cord. Similar results were obtained in TDP-43^{A315T} mice,

85   where microglial pyroptosis activation was significantly increased in the motor cortex upon

86   symptom onset, and correlated with neuronal loss. There was no significant correlation with the

87   presence of TDP-43 pathological proteins both in human and mouse tissue. Our findings

88   emphasize the importance of microglial NLRP3 inflammasome-mediated pyroptosis activation

89   for neuronal degeneration in ALS and pave the way for new therapeutic strategies counteracting

90   motor neuron degeneration in ALS by inhibiting microglial inflammasome/pyroptosis

91   activation.

92

93

94 **List of abbreviations**

95	ALRs	Absent in melanoma-like receptors
96	ALS	Amyotrophic lateral sclerosis
97	ASC	Apoptosis-associated speck-like protein containing a CARD
98	ATP	Adenosine triphosphate
99	Aβ	Amyloid beta
100	C9ORF72	Chromosome 9 open reading frame 72
101	CARD	Caspase recruitment domain
102	CERAD	Consortium to Establish a Registry for Alzheimer's disease
103	CNS	Central nervous system
104	DAMPs	Damage-associated molecular patterns
105	DAB	3,3'-Diaminobenzidine
106	FTLD	Frontotemporal lobar degeneration
107	FTD	Frontotemporal dementia
108	FTLD-TDP	Frontotemporal lobar degeneration with TDP-43 pathology
109	GAPDH	Glyceraldehyde-3-phosphate dehydrogenase
110	GSDMD	Gasdermin D
111	GSDMD-NT	Gasdermin D N-terminal region
112	HRP	Horseradish peroxidase
113	IL	Interleukin
114	IHC	Immunohistochemistry
115	MTL	Medial temporal lobe
116	NFT	Neurofibrillary tangle
117	NFκB	Nuclear factor-κB
118	NLRs	Nucleotide-binding domain and leucine-rich repeat-containing receptors
119	NLRP3	NOD-, LRR- and pyrin domain-containing protein 3
120	PAMPs	Pathogen-associated molecular patterns
121	PRP	Prion protein
122	PRRs	Pattern recognition receptors
123	pTDP-43	Phosphorylated transactive response DNA-binding protein 43kDa
124	PYD	Pyrin domain
125	ROS	Reactive oxygen species

126	SDS-PAGE	Sodium dodecyl sulfate-polyacrylamide gel electrophoresis
127	SOD1	Superoxide dismutase 1
128	TBS	Tris-buffered saline
129	TDP-43	Transactive response DNA-binding protein 43kDa
130	TLRs	Toll-like receptors
131		
132		
133		
134		
135		
136		
137		

138 **<u>Introduction</u>**

139 Amyotrophic lateral sclerosis (ALS) is a neurodegenerative disorder characterized by

140 progressive muscular paralysis resulting from degeneration of both the upper motor neurons

141 situated in the primary motor cortex, and the lower motor neurons situated in the brainstem and

142 spinal cord [17]. This rare disease affects 1-3 individuals per 100 000 per year [37, 41]. ALS

143 patients usually die due to respiratory failure within 2-5 years following disease onset [49]. In

144 approximately 10% of ALS cases there is a family history of the disease (familial ALS),

145 whereas for most of the sporadic ALS cases the cause is unknown [36]. The main pathological

146 characteristic of 97% of ALS patients is the cytoplasmic mislocalization and aggregation of

147 transactive response DNA-binding protein 43kD (TDP-43) in affected central nervous system

148 (CNS) regions [33]. TDP-43 inclusions are also found in about 50% of patients with

149 frontotemporal lobar degeneration (FTLD), referred to as FTLD-TDP [13]. It has become clear

150 that ALS and FTLD belong to a disease spectrum as up to 50% of ALS patients show some

151 features of FTLD and hexanucleotide repeat expansions in the *C9orf72* gene are the most

152 common genetic cause of ALS and FTLD [40]. Although ALS is considered a motor neuron

153 disorder, non-cell autonomous mechanisms, such as neuroinflammation, are believed to

154 significantly contribute to ALS pathogenesis. This suggests that glial cells also contribute to

155 motor neuron degeneration observed in the ALS CNS [27, 34].

156 Inflammasomes were shown to play an important role in neuroinflammation and

157 neurodegeneration. These are multiprotein complexes mainly located in immune cells, neurons,

158 microglia and astrocytes in the CNS [15]. They function as cytosolic scaffolds assembled by

159 pattern recognition receptors (PRRs) and are responsible for detecting and eliminating

160 pathogen-associated molecular patterns (PAMPs) and damage-associated molecular patterns

161 (DAMPs). The sensors of the inflammasome can be classified into three types, including

162 nucleotide-binding domain and leucine-rich repeat-containing receptors (NLRs), absent in

163 melanoma-like receptors (ALRs) and pyrin. The adaptor protein apoptosis-associated speck-

164 like protein containing a CARD (ASC) links the pyrin domain (PYD) of these sensors to the

165 caspase recruitment domain (CARD) of pro-caspase-1. However, some inflammasomes can

166 directly recruit pro-caspase-1, without the adaptor protein ASC [46]. The assembly and

167 activation of the inflammasome is cell-type and stimulus specific. The most investigated sensor

168 protein is NLRP3, which is thought to be the main sensor for sterile inflammatory stimuli, while

169 for example NLRC4 mainly acts as a sensor of bacterial infection [9, 15, 50].

170 The activation of the inflammasome through the canonical signaling pathway causes cleavage

171 of pro-caspase-1 into active caspase-1 fragments (caspase-1 p20). Subsequently, caspase-1

172 cleaves biologically inactive pro-IL-1β and pro-IL-18 into the mature inflammatory cytokines

173 IL-1β and IL-18. In addition, caspase-1 cleaves and activates Gasdermin D (GSDMD) leading

174 to the release of an N-terminal region (GSDMD-NT), which oligomerizes and binds to acidic

175 phospholipids, such as phosphoinositides on the inner part of the plasma membrane, to form

176 death-inducing pores. This causes cell swelling, rupture of the plasma membrane and the release

177 of IL-1β and IL-18 to the extracellular space, inducing the pro-inflammatory type of regulated

178 cell death known as pyroptosis. It is thought that cleaved GSDMD, which functions as the

179 effector of pyroptosis, might target and perforate multiple organelles, in addition to the plasma

180 membrane [12, 15]. Extracellular IL-18 and IL-1β can also recruit and activate other immune

181 cells, expanding the local inflammatory response. In the CNS, microglia, astrocytes and neurons

182 can all undergo pyroptosis and express its related downstream molecules and receptors, taking

183 part in the local inflammatory reaction [50].

184 The NLRP3 inflammasome has been implicated in several neurodegenerative disorders, as it

185 was shown that the inflammasome could be activated by abnormal protein aggregation,

186 including for example amyloid-β in Alzheimer's disease [19] and α-synuclein in Parkinson's

187 disease [47]. For ALS, most research related to the inflammasome and pyroptotic cell death has

188 been conducted in mutant superoxide dismutase-1 (SOD1) animal models. Multiple studies

189 showed an upregulation of the expression of several NLRP3 inflammasome components, as

190 well as the cytokines IL-18 and IL-1β, in the CNS of SOD1 mice and rats compared to controls

191 [2, 8, 16, 22]. Moreover, it was demonstrated that mutant SOD1 could activate microglia,

192 leading to caspase-1 activation and consequent cleavage of IL-1β. This was not the case when

193 microglia were deficient for NLRP3, suggesting that NLRP3 is the key inflammasome in

194 mediating SOD1-induced microglial pyroptosis activation [10, 29]. For TDP-43, there is

195 evidence that mutant and aggregated forms of TDP-43 can trigger NLRP3 inflammasome-

196 dependent IL-1β and IL-18 secretion *in vitro* in microglia, which was toxic to motor neurons

197 [25, 53]. In the absence of microglia, TDP-43 was not toxic to motor neurons [53]. Whether

198 this NLRP3 inflammasome-related microglia activation as observed in mouse models and *in*

199 *vitro* aggregation models plays a role in sporadic ALS patients, and whether this is related to

200 TDP-43 pathology and neuronal degeneration, remains unclear.

201

202   **<u>Materials and Methods</u>**

203   **Human autopsy cases**

204   Brain and spinal cord tissue was collected in accordance with the applicable laws in Belgium

205   (UZ Leuven) and Germany (Ulm). The recruitment protocols for collecting the brains were

206   approved by the ethical committees of the University of Ulm (Germany) and UZ Leuven

207   (Belgium). This study was approved by the UZ Leuven ethical committee (Belgium). Tissues

208   were collected with an average *post-mortem* interval of 44 h. After autopsy, the right

209   hemisphere was dissected in coronal planes and frozen at -80°C. The left hemisphere was fixed

210   in 4% phosphate-buffered formaldehyde. 25 ALS cases (15 sporadic and 10 *C9orf72*) and 19

211   non-neurodegenerative controls were included in this study (Suppl. Table 1, online resource).

212   The diagnosis of ALS or FTD was based on clinical assessment according to the consensus

213   criteria for ALS [4–6] and FTD [14, 35]. The *post-mortem* diagnosis of ALS and FTLD-TDP

214   was pathologically confirmed by assessment of the pTDP-43 pathology. Braak NFT stage [3],

215   AβMTL phase [42], and the Consortium to Establish a Registry for Alzheimer's disease

216   (CERAD) score [31] were determined based on immunohistochemical stainings with antibodies

217   against Aβ and abnormally phosphorylated tau protein (p-tau) (Suppl. Table 2, online

218   resource).

219   *C9orf72* **repeat expansion determination**

220   DNA was extracted from peripheral blood and/or cerebellum according to standard protocols.

221   Analysis of the hexanucleotide repeat length in intron 1 of *C9orf72* was performed by fragment

222   length analysis by PCR and repeat-primed PCR (RP-PCR) as previously described [7]. In

223   addition, the presence of poly(GA) pathology was immunohistochemically assessed in the

224   frontal cortex. The *C9orf72* mutation status is shown in Suppl. Table 1 (online resource).

225

Transgenic mice

226

227 Heterozygous mice overexpressing a TDP-43 construct containing the A315T mutation driven

228 by the mouse prion protein (Prp) promotor (Prp-hTDP-43[A315T]) were used in this study [48].

229 Transgenic mice were bred by continuous backcrossing of heterozygous males with wild-type

230 females on a C57BL/6 background. Due to intestinal obstruction problems in this model, the

231 animals were given gel food from the age of two months onwards (DietGel®31M, ClearH2O,

232 Portland, ME, US), which is known to overcome this problem [20]. Five groups of mice (total

233 n = 28) were used: (1) wild-type non-transgenic mice at six months of age (n = 3), (2) Prp-

234 hTDP-43[A315T] mice at six months of age (n = 4), (3) non-transgenic mice at 16 months of age

235 (n = 4), (4) Prp-hTDP-43[A315T] mice at 16 months of age (n = 7), and (5) symptomatic Prp-

236 hTDP-43[A315T] mice (n = 5; 6-14 months of age, mean age of 9 months). In group 5, mice were

237 sacrificed 1-3 days following symptom onset, i.e., detection of impaired and reduced movement

238 in the cage. Mouse brains and spinal cords were harvested after death and fixed in 4%

239 paraformaldehyde for three to five days. After paraffin embedding, sections of 5 µm were cut

240 with a microtome and used for immunohistochemistry. All animal care and experiments were

241 approved by the KU Leuven Ethical Committee and were carried out according to the Belgian

242 law.

Immunohistochemistry

243

244 <u>Human samples</u>

245 Five µm thick sections were cut from formalin-fixed, paraffin-embedded tissue of motor cortex

246 and spinal cord. Sections were stained with antibodies against pTDP-43, Aβ, p-tau, cleaved

247 GSDMD, caspase-1, IL-18, ASC and NLRP3 (Suppl. Table 2, online resource). Stainings were

248 performed with the BOND-MAX automated IHC/ISH Stainer (Leica Biosystems, Wetzlar,

249 Germany) using the Bond Polymer Refine Detection kit (DS9800, Leica Biosystems). Briefly,

250 slides were deparaffinized and epitopes were retrieved with low or high pH buffer. After

251 incubation with Envision Flex Peroxidase-Blocking Reagent (Dako, Glostrup, Denmark), slides

252 were incubated with primary antibodies for 30 min, followed by secondary antibody incubation.

253 DAB was used for visualization. Counterstaining with hematoxylin was carried out, followed

254 by dehydration and mounting in an automated cover-slipper (Leica Biosystems). Images were

255 acquired using the Leica DM2000 LED microscope coupled to a Leica DFC 7000 T camera.

256 Images were processed using ImageJ and combined into figures using Inkscape.

257 For immunofluorescence double labeling using primary antibodies from different species

258 (Suppl. Table 2, online resource), an antibody cocktail of the respective primary antibodies was

259 applied, followed by a cocktail of species-specific Cy2/3-conjugated secondary antibodies

260 (Jackson ImmunoResearch, Ltd, West Grove, PA, USA). For double labeling with primary

261 antibodies raised in the same species (Suppl. Table 2, online resource), a sequential staining

262 was performed using a rabbit-on-rabbit staining protocol as previously described [45]. Briefly,

263 a coupling method was used to avoid cross-reactivity of secondary antibodies. The first rabbit

264 primary antibody was used as described above, followed by a Cy2-labelled donkey anti-rabbit

265 secondary antibody. The second rabbit primary antibody was coupled to a donkey anti-rabbit

266 Fab fragment conjugated to a Cy3 dye for 20 min (2 µg Fab fragment per 1 µg primary antibody)

267 prior to its incubation with the sample. Next, normal rabbit serum (Jackson ImmunoResearch)

268 was added for another 10 min to capture the unbound Fab fragments (10 µl serum per 1 µg Fab

269 fragment). Then, the mix was applied to the slides to visualize the second primary antibody.

270 TrueBlack Lipofuscin Autofluorescence Quencher (Biotum, CA, USA) was applied for 30s to

271 reduce autofluorescence. Fluorescent-labelled slides were mounted using ProLong Gold

272 Antifade Mountant containing DAPI (Thermo Fisher Scientific, Rockford, IL, USA) for

273 counterstaining of the nuclei. Images were acquired with a Leica SP8x confocal microscope

274 (Leica Microsystems, Wetzlar, Germany) at a magnification of 63x using type F immersion oil

275   (Leica Microsystems). Images were processed using ImageJ and combined into figures using

276   Inkscape.

277   <u>Mouse samples</u>

278   Mouse brain sections were stained with antibodies against TDP-43, ubiquitin, GSDMD,

279   caspase-1 and Iba1 (Suppl. Table 2, online resource). Stainings were performed manually,

280   similar to immunohistochemistry and immunofluorescence of the human slides. An extra mouse

281   IgG blocking step was performed to prevent unspecific signal. For GSDMD, proteinase K

282   treatment was additionally applied for 1 min.

283   **pTDP-43 pathology and TDP-43 nuclear clearance quantification in human samples**

284   pTDP-43 pathology was assessed in the motor cortex and the anterior horn of the lumbosacral

285   spinal cord of human cases. The amount of pathological inclusions in a 20x microscopic field

286   with most abundant pathology, considered as the "hotspot area", was quantified. The abundance

287   of pathology was expressed as a percentage of neurons affected by pTDP-43 pathology. For

288   quantification of the percentage of neurons with TDP-43 cleared form the nucleus in layer V of

289   the motor cortex, two images (0.632 x 0.474 mm) of anti-TDP-43 (C-terminal) stained sections

290   were taken using a 20x objective. Image J was used for quantifications. The percentage of

291   neurons without TDP-43 in the nucleus was calculated in relation to all neurons present in the

292   respective region of interest.

293   **TDP-43 nuclear clearance quantification in mouse samples**

294   For quantification of the percentage of neurons with TDP-43 cleared from the nucleus in the

295   motor cortex and anterior horn of the spinal cord of all mice, two images (0.632 x 0.474 mm)

296   of anti-TDP-43 (C-terminal) stained sections were taken with the Leica DM2000 LED

297   microscope using a 20x objective. Image analysis was performed using ImageJ. The percentage

298 of neurons without TDP-43 in the nucleus was calculated in relation to all neurons present in

299 the respective region of interest.

300 **Quantification of number of cleaved GSDMD- and caspase-1-positive glia / neurons**

301 <u>Human samples</u>

302 For quantification of the number of cleaved GSDMD- and caspase-1-positive microglial cells

303 and neurons in the precentral white matter and in layer V of the motor cortex, three consecutive

304 images (0.632 x 0.474 mm) of anti-cleaved GSDMD- and anti-caspase-1-stained sections were

305 taken with the Leica DM2000 LED microscope using a 20x objective. For the lumbar spinal

306 cord ventral pyramidal tracts, one 20x image was acquired, while for the lateral pyramidal tracts

307 two 20x images were used. For the lumbar spinal cord anterior horn, two 10x images (1.264 x

308 0.948 mm) were used. Microglial cells were identified by their shape and nuclear morphology.

309 Image analysis was performed using ImageJ.

310 <u>Mouse samples</u>

311 For quantification of the number of microglial cells positive for GSDMD and caspase-1 per

312 mm² in the motor cortex (gray and white matter) and spinal cord (anterior horn and pyramidal

313 tracts) of all mice, four images (0.632 x 0.474 mm) of anti-GSDMD- and anti-caspase-1-stained

314 sections were taken with the Leica DM2000 LED microscope using a 20x objective. Microglial

315 cells were identified by their shape and nuclear morphology. Image analysis was performed

316 using ImageJ.

317 **Quantification of neuronal density in the motor cortex and spinal cord**

318 <u>Human samples</u>

319 For quantification of neuronal density in layer V of the motor cortex, three consecutive images

320 (0.632 x 0.474 mm) of a representative area of anti-cleaved GSDMD-stained sections were

321   taken with the Leica DM2000 LED microscope using a 20x objective [24]. For quantification

322   of neuronal density in the anterior horn of the lumbosacral spinal cord, two images (1.264 x

323   0.948 mm) of a representative area of anti-cleaved GSDMD-stained sections were taken using

324   a 10x objective. Criteria regarding morphological conditions of neurons to be included were

325   determined before quantification. Neurons were identified based on their nuclear pattern in the

326   hematoxylin staining. Image analysis was performed using ImageJ.

327   <u>Mouse samples</u>

328   For quantification of neuronal density in layer V of the motor cortex and in the anterior horn of

329   the spinal cord, two images (0.632 x 0.474 mm) of anti-TDP-43-stained sections were taken

330   with the Leica DM2000 LED microscope using a 20x objective. Criteria regarding

331   morphological conditions of neurons to be included were determined before quantification,

332   similar as for the human samples. Image analysis was performed using ImageJ.

333   **Protein extraction**

334   For biochemistry, the spinal cord was taken and the right brain hemisphere was cut in approx.

335   1 cm thick slabs and frozen at -80°C. Fifty mg of brain or spinal cord tissue was weighed and

336   mechanically homogenized in 0.5 ml 2% SDS in TBS (Tris-buffered saline) with Nuclease

337   (Pierce^{TM} Universal Nuclease, Thermo Fisher Scientific) and a cocktail of protease/phosphatase

338   inhibitors (Halt, Thermo Fisher Scientific) using a micropestle. Samples were sonicated,

339   followed by a centrifugation at 14 000 *g* for 30 min. The resulting supernatant was used. Protein

340   concentrations were determined using the Pierce BCA Protein Assay Kit (Thermo Fisher

341   Scientific).

342   **Western blotting**

343   For western blotting, 10 μg of protein was loaded on a Bis-Tris 4-12% gradient SDS-PAGE

344   (Invitrogen, Thermo Fisher Scientific) in MOPS/MES-SDS running buffer (Alfa Aesar,

345   Haverhill, MA, USA), electrophoresed at 150V for 60 min, and transferred to a nitrocellulose

346   membrane (Semidry transfer, Biorad, Hercules, CA, USA). Membranes were blocked with 5%

347   non-fat dried milk (AppliChem, Darmstadt, Germany) in PBS 0.1% Tween-20 (PBST). Primary

348   antibodies and the corresponding dilutions are listed in Suppl. Table 2 (online resource).

349   Secondary antibodies were goat anti-rabbit IgG-HRP or goat anti-mouse IgG-HRP (1:10 000,

350   polyclonal, Dako). Blots were developed with SuperSignal West Pico or Dura plus ECL reagent

351   (Thermo Fisher Scientific). Digital images were acquired using the Amersham Imager 600 (GE

352   Healthcare, Chicago, IL, USA). All blots were stripped (Restore Western Blot Stripping Buffer,

353   Thermo Fisher Scientific) of bound antibodies and reprobed with GAPDH to control for equal

354   protein loading. Band intensities were measured using ImageJ and were normalized to GAPDH.

355   **Statistical analysis**

356   Statistical analyses were performed using IBM SPSS and Graphpad Prism software. Binary

357   logistic regression controlled for age and sex, or a t-test or Mann-Whitney test were used to

358   determine the significant difference between two groups. To examine the different mouse

359   groups, a one-way ANOVA or Kruskal-Wallis test was used followed by a post-hoc test to

360   correct for multiple testing. To examine correlations between motor cortex layer V neuronal

361   density or anterior horn spinal cord neuronal density and several parameters, partial Pearson's

362   correlation analysis (controlled for age and sex for the human cohort) was performed. To

363   estimate the effect of explanatory variables on human motor cortex layer V neuronal density,

364   we conducted linear regression analyses. Data are presented as mean ± SEM. * $p < 0.05$; ** p

365   < 0.01; *** $p < 0.001$; **** $p < 0.0001$.

366

367

368   **Results**

369   **The canonical NLRP3 inflammasome as well as pyroptosis effector-related proteins are**

370   **expressed in microglial cells in the ALS motor cortex**

371   To investigate the expression of NLRP3 inflammasome components in the ALS brain, we

372   performed a pathological analysis on human *post-mortem* brain tissue from ALS (n = 24) and

373   control (n = 12) cases (Suppl. Table 1, online resource). For this, we used motor cortex, as this

374   is the main affected brain region in ALS. Immunohistochemical staining showed positive

375   immunoreactivity for NLRP3 (Fig. 1a), ASC (Fig. 1f) and caspase-1 (Fig. 1k) in microglial

376   cells in the ALS motor cortex and its adjacent white matter. This was also observed in some

377   control cases for ASC and caspase-1, and to a lesser extent for NLRP3 (Suppl. Fig. 1a-c, online

378   resource). To further confirm that the inflammasome was expressed in microglia, we performed

379   immunofluorescence co-staining with an antibody against Iba1 for microglia. This ensured the

380   expression of NLRP3 (Fig. 1b-e), ASC (Fig. 1g-j) and caspase-1 (Fig. 1l-o) in microglial cells

381   in the ALS motor cortex white and gray matter.

382   Next, we assessed the expression of pyroptosis effector-related proteins in the ALS motor

383   cortex. Both cleaved GSDMD (Fig. 1p) and IL-18 (Fig. 1u) were present in ALS microglial

384   cells, as shown by DAB immunohistochemistry. Control cases showed a few microglial cells

385   positive for cleaved GSDMD and IL-18, but these seemed scarcer compared to ALS cases

386   (Suppl. Fig. 1d-e, online resource). Immunofluorescence co-staining confirmed that these

387   effector proteins were present in Iba1-positive microglial cells (Fig. 1 q-t and v-y), but not in

388   astrocytes and oligodendrocytes, as shown by GFAP and Olig2 antibody staining respectively

389   (Suppl. Fig. 2, online resource). Of note, antibodies against cleaved GSDMD, NLRP3 and IL-

390   18 also faintly stained few neurons. No positive neurons were observed for ASC and caspase-

391   1 (Table 1). Astrocytes were rarely positive for NLRP3, caspase-1 and cleaved GSDMD, and

392   negative for ASC and IL-18. Oligodendrocytes were negative for all inflammasome and

393   pyroptosis effector protein markers (Table 1).

Increased presence of cleaved GSDMD-positive microglial cells in ALS precentral white

matter correlates with neuronal loss

396   To determine whether the expression of pyroptosis-related proteins is relevant for ALS, we

397   quantified the amount of microglia in the motor cortex positive for caspase-1 (inflammasome

398   component) and cleaved GSDMD (pyroptosis effector). Caspase-1 was selected as

399   inflammasome marker as this protease is responsible for the cleavage and consequent activation

400   of downstream pyroptosis targets (i.e. GSDMD, IL-18 and IL-1β), while cleaved GSDMD was

401   used as a marker for pyroptosis activation, as it is considered the final executor of pyroptotic

402   cell death. In layer V of the motor cortex, we detected a decrease in the number of caspase-1-

403   positive microglia in ALS cases compared to controls (Fig. 2a; Suppl. Table 3, online resource;

404   $p = 0.031$; OR = 0.975; 95% CI = 0.954-0.998; binary logistic regression corrected for age and

405   sex). We did not observe any differences between ALS and control cases regarding cleaved

406   GSDMD-positive microglia (Fig. 2b; Suppl. Table 3, online resource; $p = 0.345$; OR = 1.138;

407   95% CI = 0.870-1.488; binary logistic regression corrected for age and sex). There was also no

408   difference in the number of neurons in layer V of the motor cortex gray matter positive for

409   cleaved GSDMD (Suppl. Fig 3; Suppl. Table 3, online resource; $p = 0.527$; OR = 0.988; 95%

410   CI = 0.952-1.025; binary logistic regression corrected for age and sex). In the precentral white

411   matter, there was no difference in the number of caspase-1-positive microglia between ALS and

412   control cases (Fig. 2c; Suppl. Table 3, online resource; $p = 0.4$; OR = 1.006; 95% CI = 0.992-

413   1.020; binary logistic regression corrected for age and sex). Interestingly, ALS cases showed a

414   higher abundance of microglia positive for cleaved GSDMD compared to control cases in the

415   precentral white matter (Fig. 2d; Suppl. Table 3, online resource; $p = 0.034$; OR = 1.155; 95%

416   CI = 1.011-1.319; binary logistic regression corrected for age and sex).

417 To examine whether the expression of pyroptosis-related proteins correlates with neuronal loss

418 in ALS, we quantified neuronal densities in layer V of the motor cortex of ALS and control

419 cases. Binary logistic regression corrected for age and sex showed a decrease in motor cortex

420 layer V neuronal density in ALS compared to control cases (Fig. 3a; Suppl. Table 3, online

421 resource; $p = 0.023$; OR = 0.880; 95% CI = 0.788-0.982). Additionally, we detected a

422 significantly higher percentage of neurons affected by pTDP-43 pathology in ALS compared to

423 control motor cortex (Fig. 3b; $p = 0.007$; Mann-Whitney test), and a significantly higher

424 percentage of neurons with TDP-43 cleared from the nucleus in layer V of the motor cortex

425 (Fig. 3c; Suppl. Table 3, online resource; $p = 0.022$; OR = 1.179; 95% CI = 1.023-1.358; binary

426 logistic regression corrected for age and sex). A Pearson's partial correlation analysis corrected

427 for age and sex revealed a significant correlation between the percentage of pTDP-43 affected

428 neurons and a decreased motor cortex layer V neuronal density (Table 2; r = -0.504; $p = 0.007$).

429 Interestingly, a decreased motor cortex layer V neuronal density correlated with a higher

430 abundance of white matter microglia positive for cleaved GSDMD (Table 2; r = -0.431; $p = $

431 0.025). In contrast, layer V neuronal density did not significantly correlate with the number of

432 white matter microglia positive for caspase-1 (Table 2; r = -0.343; $p = 0.080$). There was also

433 no correlation between cleaved GSDMD- and caspase-1-positive white matter microglia (Table

434 2; r = 0.020; $p = 0.921$). The amount of cleaved GSDMD-positive white matter microglia did

435 not correlate with the percentage of pTDP-43 affected neurons (Table 2; r = -0.010; $p = 0.960$),

436 nor with the percentage of neurons with TDP-43 nuclear clearance (Table 2; r = 0.116; $p = $

437 0.572). In separate linear regression models with motor cortex layer V neuronal density as

438 dependent variable, and including age and sex as extra independent variables, the percentage of

439 neurons affected by pTDP-43 pathology ($\beta = -0.435$; $p = 0.01$) and the number of cleaved

440 GSDMD-positive white matter microglia ($\beta = -0.455$; $p = 0.021$) were good predictors of

441 neuronal density, whereas the number of caspase-1-positive white matter microglia was not (β

442   = -0.244; $p = 0.179$) (Suppl. Table 4, part 1, online resource). When combining the percentage

443   of pTDP-43 affected neurons and cleaved GSDMD-positive white matter microglia in the same

444   model, both showed to be equally potent predictors of motor cortex layer V neuronal density

445   (Suppl. Table 4, part 2, online resource; percentage of pTDP-43 affected neurons: $\beta = -0.486$;

446    $p = 0.004$; cleaved GSDMD-positive white matter microglia: $\beta = -0.464$; $p = 0.007$), indicating

447   that they independently contribute to neuronal loss.

Elevated expression of pyroptosis-related proteins in ALS motor cortex

449   To further investigate the expression of pyroptosis-related proteins in ALS versus control motor

450   cortex, we performed western blots on SDS-soluble motor cortex extracts. ALS cases showed

451   an increased expression of the inflammasome component full length caspase-1 (Fig. 4a,b;

452   Suppl. Fig. 4a, online resource; $p < 0.0001$; unpaired t-test) as well as the active cleaved p20

453   fragment (Fig. 4a,c; Suppl. Fig. 4a, online resource; $p = 0.0001$; unpaired t-test). Expression of

454   cleaved GSDMD, which represents the active cleaved fragment of GSDMD, was numerically

455   increased in ALS cases, however not significant (Fig. 4a,d; Suppl. Fig. 4b, online resource; $p = $

456   0.2568; unpaired t-test). Finally, the expression of the cleaved and active form of IL-18 was

457   significantly increased in the motor cortex of ALS compared to control cases (Fig. 4a,e; Suppl.

458   Fig. 4c, online resource; $p < 0.0001$; unpaired t-test).

Presence of NLRP3 inflammasome and pyroptosis-related proteins in the ALS spinal cord

does not associate with neuronal loss

461   Next, we assessed the presence of the inflammasome component caspase-1 and the pyroptosis

462   effector cleaved GSDMD in the ALS spinal cord. We analyzed the amount of microglia positive

463   for caspase-1 and cleaved GSDMD in the ventral and lateral white matter pyramidal tracts.

464   There was no obvious difference between ALS and control cases in the number of caspase-1-

465   positive microglia in the ventral pyramidal tracts (Fig. 5a; Suppl. Table 3, online resource; $p = $

466 0.270; OR = 0.947; 95% CI = 0.860-1.043; binary logistic regression corrected for age and sex)

467 and in the lateral pyramidal tracts (Fig. 5c; Suppl. Table 3, online resource; $p = 0.606$; OR =

468 1.002; 95% CI = 0.994-1.010; binary logistic regression corrected for age and sex). The number

469 of cleaved GSDMD-positive microglia was numerically slightly higher in ALS compared to

470 control cases for the ventral pyramidal tracts (Fig. 5b; Suppl. Table 3, online resource; $p =$

471 0.216; OR = 1.285; 95% CI = 0.864-1.912; binary logistic regression corrected for age and sex),

472 and for the lateral pyramidal tracts (Fig. 5d; Suppl. Table 3, online resource; $p = 0.172$; OR =

473 1.086; 95% CI = 0.965-1.224; binary logistic regression corrected for age and sex).

474 We also quantified the anterior horn neuronal density and the percentage of neurons affected

475 by pTDP-43 pathology in the spinal cord of ALS and control cases. As expected, the anterior

476 horn neuronal density was significantly lower in ALS compared to control cases (Suppl. Fig.

477 5a; Suppl. Table 3, online resource; $p = 0.017$; OR = 0.912; 95% CI = 0.846-0.984; binary

478 logistic regression corrected for age and sex), while the percentage of pTDP-43 affected neurons

479 was increased (Suppl. Fig. 5b, online resource, $p < 0.0001$; Mann-Whitney test). A Pearson's

480 partial correlation corrected for age and sex did not indicate any correlation between the number

481 of cleaved GSDMD-positive microglia in the lateral pyramidal tracts and the anterior horn

482 neuronal density (Suppl. Table 5, online resource; r = 0.045; $p = 0.832$), nor with the percentage

483 of pTDP-43 affected neurons (Suppl. Table 4, online resource; r = 0.208; $p = 0.318$). However,

484 the anterior horn neuronal density correlated with the percentage of neurons affected by pTDP-

485 43 pathology, similar to our observations in the motor cortex (Suppl. Table 5, online resource;

486 r = -0.544; $p = 0.004$).

487 Finally, we biochemically assessed the expression of pyroptosis-related proteins in the spinal

488 cord of ALS and control cases. ALS SDS-soluble spinal cord extracts displayed an increased

489 expression of full-length caspase-1 (Fig. 6a,b; Suppl. Fig. 6a, online resource; $p = 0.0134$;

490 unpaired t-test), as well as the cleaved and active p20 fragment (Fig. 6a,c; Suppl. Fig. 6a, online

491   resource; $p = 0.0002$; unpaired t-test). Additionally, we detected an increased expression of

492   pyroptosis effector proteins cleaved GSDMD (Fig. 6a,d; Suppl. Fig. 6b, online resource; $p =$

493   0.0003; unpaired t-test) and IL-18 (Fig. 6a,e; Suppl. Fig. 6c, online resource; $p = 0.0022$; Mann-

494   Whitney test).

495   **Increased GSDMD reactivity in symptomatic TDP-43^{A315T} transgenic mice is associated**

496   **with a decreased neuronal density in the brain**

497   To explore whether the pyroptosis pathway was also activated in animal models of ALS, we

498   investigated the presence of the inflammasome component caspase-1 and the pyroptosis

499   effector protein GSDMD in the brain and spinal cord of TDP-43^{A315T} transgenic mice. We

500   detected microglia positive for caspase-1 (Fig. 7a; Suppl. Fig. 7a-d, online resource) and

501   GSDMD (Fig. 7b; Suppl. Fig. 7e-h, online resource) in the gray and white matter of the motor

502   cortex and spinal cord of symptomatic TDP-43^{A315T} transgenic mice. We quantified the number

503   of caspase-1- and GSDMD-positive microglia per mm² in the motor cortex and in the spinal

504   cord (gray + white matter) in five different mouse groups: (1) 6 months old wild-type mice, (2)

505   16 months old wild-type mice, (3) 6 months old TDP-43^{A315T} transgenic mice, (4) 16 months

506   old TDP-43^{A315T} transgenic mice, and (5) symptomatic TDP-43^{A315T} transgenic mice (6-14

507   months old, mean age of 9 months old). In the motor cortex, the number of caspase-1-positive

508   microglia was significantly increased in 16 months old wild-type and 16 months old TDP-

509   43^{A315T} transgenic mice compared to their 6 months old counterparts (Fig. 7c; wild-type: $p =$

510   0.0289; TDP-43^{A315T} transgenic: $p = 0.0149$; one-way ANOVA followed by Tukey's multiple

511   comparisons). The number of caspase-1-positive microglia was not increased in the brain of

512   symptomatic TDP-43^{A315T} transgenic mice. In contrast, the amount of GSDMD-positive

513   microglia was significantly increased in symptomatic TDP-43^{A315T} transgenic compared to 6

514   months old wild-type mice (Fig. 7d; $p = 0.0014$; one-way ANOVA followed by Tukey's

515   multiple comparisons), 16 months old wild-type mice ($p = 0.0039$); 6 months old TDP-43^{A315T}

516 transgenic mice ($p = 0.0006$) and 16 months old TDP-43^{A315T} transgenic mice ($p = 0.0041$). In

517 the spinal cord, a similar increase in caspase-1-positive microglia was detected as in the brain

518 in 16 months old wild-type and TDP-43^{A315T} transgenic mice, although not significant (Fig. 7e).

519 Symptomatic TDP-43^{A315T} transgenic mice showed similar levels of caspase-1-positive

520 microglia in the spinal cord compared to the 16 months old groups. Finally, we analyzed the

521 amount of GSDMD-positive microglia in the spinal cord. Similar to as was observed in the

522 brain, this was significantly increased in symptomatic TDP-43^{A315T} transgenic mice compared

523 to 6 months old wild-type mice (Fig. 7f; $p = 0.0267$; Kruskal-Wallis test followed by Dunn's

524 multiple comparisons), 16 months old wild-type mice ($p = 0.0133$), and 16 months old TDP-

525 43^{A315T} transgenic mice ($p = 0.0038$).

526 Next, we focused on TDP-43, as this protein is mutated in the mouse model. No typical

527 cytoplasmic TDP-43-positive inclusions were observed, although symptomatic TDP-43^{A315T}

528 transgenic mice occasionally displayed dense aggregated material around the nucleus positive

529 for TDP-43 (Suppl. Fig. 8a, online resource; arrow), while the nucleus was not stained. Nuclear

530 clearance of physiological TDP-43 was a prominent phenotype, which we quantified for the

531 different mouse groups. In the motor cortex, TDP-43 nuclear clearance was significantly

532 increased in symptomatic TDP-43^{A315T} transgenic mice compared to 16 months old wild-type

533 mice (Suppl. Fig. 8a,c, online resource; $p = 0.006$; Kruskal-Wallis test followed by Dunn's

534 multiple comparisons). We also noticed a numerical but non-significant increase in the 16

535 months old TDP-43^{A315T} transgenic group. In the spinal cord anterior horn, no differences in

536 TDP-43 nuclear clearance could be detected among the groups (Suppl. Fig. 8b,d, online

537 resource).

538 We further analyzed the different mouse groups immunohistochemically using an antibody

539 against ubiquitin, as it was previously shown that ubiquitin-positive but TDP-43-negative

540 material could be detected in this model [48]. We observed diffuse cytoplasmic ubiquitin-

541   positive staining in neurons both in the motor cortex (Suppl. Fig. 9a, online resource) and in the

542   spinal cord (Suppl. Fig. 9b, online resource) of the majority of symptomatic TDP-43^{A315T}

543   transgenic mice. This ubiquitin-positive neuronal staining was also observed in one 6-months-

544   old and two 16-months-old TDP-43^{A315T} transgenic asymptomatic mice. An antibody against

545   SQSTM1/p62 displayed a similar neuronal staining pattern, for the first time indicating that

546   affected neurons in symptomatic TDP-43^{A315T} transgenic mice are positive for SQSTM1/p62

547   (Suppl. Fig. 9c,d, online resource). Finally, we assessed the neuronal density in layer V of the

548   motor cortex and the anterior horn of the spinal cord of the different mouse groups to evaluate

549   whether neuronal loss was present in the model. Neuronal density was significantly decreased

550   in the motor cortex of symptomatic TDP-43^{A315T} transgenic mice compared to 6 months old

551   wild-type mice (Suppl. Fig. 10a, online resource; $p = 0.0307$; Kruskal-Wallis test followed by

552   Dunn's multiple comparisons). In the spinal cord, a slight but non-significant decrease was

553   observed in the symptomatic TDP-43^{A315T} transgenic mice (Suppl. Fig. 10b, online resource).

554   Using Pearson's partial correlation analysis, we found that the number of GSDMD-positive

555   microglia in the brain significantly correlated with a decrease in motor cortex layer V neuronal

556   density (Table 3; r = -0.478; $p = 0.021$). This was not the case for caspase-1-positive microglia

557   (Table 3; r = -0.378; $p = 0.075$). The percentage of TDP-43 nuclear clearance highly correlated

558   with layer V neuronal density (Table 3; r = -0.692; $p < 0.0001$). There was also a trend towards

559   a correlation between the amount of GSDMD-positive microglia and the percentage of TDP-43

560   nuclear clearance, although not significant (Table 3; r = 0.408; $p = 0.053$). A similar analysis

561   for the spinal cord did not show any significant correlations for the abovementioned parameters

562   (Suppl. Table 6, online resource).

563

564

565

Discussion

Here, we described the expression of the NLRP3 inflammasome complex comprising of NLPR3, ASC and caspase-1, as well as pyroptosis effector-related proteins cleaved GSDMD and IL-18 in microglial cells in the ALS motor cortex and spinal cord. The microglial expression of cleaved GSDMD in the precentral white matter correlated with neuronal loss in layer V of the motor cortex, but not with the amount of pTDP-43 pathology. In the spinal cord, no increase in microglial cleaved GSDMD was detected, although elevated expression of pyroptosis-related proteins was detected biochemically both in the motor cortex and in the spinal cord (Table 4). Importantly, we observed increased GSDMD expression in microglia in the brain and spinal cord of symptomatic TDP-43^{A315T} transgenic mice, which also correlated with neuronal loss in layer V of the motor cortex, similar to our observations in human tissue. To our knowledge, this is the first time that expression of the full NLRP3 inflammasome and, importantly, the pyroptosis effector-related proteins cleaved GSDMD and IL-18 was observed in ALS microglial cells and was linked to neuronal degeneration, both in human *post-mortem* tissue and TDP-43 transgenic mice.

In human ALS brain, we observed a correlation of the abundance of pTDP-43 pathology with neuronal loss, but not with cleaved GSDMD-positive white matter microglia although the latter lesions are also associated with motor cortex neuron loss. This suggests that the presence of pTDP-43 aggregates does not directly influence the activation of pyroptosis in white matter microglia. However, this is an end-point observation, and it is possible that during the course of the disease, pathological pTDP-43, soluble or aggregated, does serve as a trigger for inflammasome and pyroptosis activation. Evidence supports the activation of the NLRP3 inflammasome by abnormal protein aggregates in neurodegenerative diseases [19, 52]. This activation requires a two-step process. First, the NFκB pathway is activated through stimulation of toll-like receptors (TLRs), leading to upregulation of the expression of NLRP3, pro-caspase-

591   1 and pro-interleukins. Secondly, the NLRP3 inflammasome can be assembled and activated

592   by a variety of stimuli, such as reactive oxygen species (ROS), extracellular ATP, lysosomal

593   rupture, low intracellular K^+, and aggregated or misfolded proteins [15, 39, 54]. Regarding

594   ALS, *in vitro* studies showed that pathological TDP-43 could induce an NLRP3-dependent

595   secretion of active IL-1β and IL-18 in microglia [10, 25, 53]. This pro-inflammatory cascade

596   was shown to be toxic to motor neurons, while in the absence of microglia, pathological TDP-

597   43 was not detrimental to motor neurons [53]. Similar results were obtained with mutant SOD1,

598   which was shown to trigger the NLRP3-dependent cleavage of caspase-1 and IL-1β in primary

599   mouse microglia [10]. These results support the hypothesis that pathological ALS proteins can

600   induce pyroptosis activation in microglia. In recent years, several groups also demonstrated an

601   upregulation of NLRP3, ASC, caspase-1, IL-1β and IL-18 in SOD1^{G93A} mice and rats [2, 8, 10,

602   16, 22, 29], which are the most commonly used animal models for ALS, although SOD1

603   mutations only explain 2% of ALS cases [43]. Deora and colleagues also showed increased

604   expression of the NLRP3 inflammasome in TDP^{Q331K} mutant mice [10]. Furthermore, TDP-43

605   was shown to interact with NFκB and to function as a suppressor of the NFκB pathway, with a

606   loss of TDP-43 leading to increased activation of the NFκB pathway [55]. This suggests that a

607   loss of nuclear TDP-43, as observed in ALS, could make cells more susceptible for pyroptosis

608   activation through a reduced inhibition of the NFκB pathway. Although the above data indicate

609   the importance of pathological TDP-43 and SOD1 in eliciting pyroptosis activation, it is likely

610   that other pathological conditions often observed in ALS (e.g. ROS, extracellular ATP), which

611   could be downstream of SOD1 and TDP-43 mutations, are responsible for NLRP3

612   inflammasome activation.

613   In human ALS cases, the abundance of cleaved GSDMD-positive microglia in the precentral

614   white matter correlated with a decreased neuronal density in layer V of the motor cortex.

615   Following pyroptosis activation, GSDMD-NT oligomerizes and associates with the plasma

616 membrane to form micropores, resulting in potassium efflux, intracellular and extracellular ion

617 imbalance, cell swelling and rupture of the plasma membrane [39]. This causes massive leakage

618 of pro-inflammatory cytokines, such as IL-1β and IL-18, as well as other cytosolic components

619 [15, 50]. In turn, IL-1β and IL-18 bind their respective receptors on glial cells and neurons,

620 initiating a complex spectrum of signaling pathways, further enhancing inflammatory responses

621 and resulting in neuronal injury and death [39]. Therefore, it is likely that the observed

622 activation of the pyroptosis pathway in ALS white matter microglia contributes to neuronal

623 degeneration in the motor cortex, possibly by affecting axonal health. However, it remains

624 unclear whether this is the primary insult in neurodegeneration, or just one contributing factor

625 enhancing neuronal toxicity among others. Importantly, the number of microglia in the human

626 white matter is significantly higher compared to gray matter [26]. Furthermore, a clear

627 difference in the immune regulatory profile was identified between white and gray matter

628 microglia, with white matter microglia displaying an increased expression of genes involved in

629 the NFκB pathway [44]. This could make white matter microglia more susceptible for

630 pyroptosis activation as activation of the NFκB pathway induces elevated expression of

631 pyroptosis-related genes, possibly explaining the increased abundance of cleaved GSDMD-

632 positive microglia specifically in the ALS precentral white matter.

633 We did not observe obvious TDP-43 pathological aggregates in the brain and spinal cord of

634 symptomatic TDP-43^{A315T} mice, although a few ubiquitin-positive neurons were detected in

635 symptomatic TDP-43^{A315T} mice, and to a lesser extent in 6 and 16 months old TDP-43^{A315T}

636 mice. This is in line with previous reports [18, 20, 48]. In the motor cortex of symptomatic

637 TDP-43^{A315T} mice, we detected an increased TDP-43 nuclear clearance. This did not

638 significantly correlate with the amount of GSDMD-positive microglia, similar to our

639 observations in the human brain. Importantly, a decrease in neuronal density in layer V of the

640 motor cortex correlated with an increased presence of GSDMD-positive microglia, mirroring

641 our human data. Others also detected a decreased number of neurons in layer V of the motor

642 cortex [48, 51]. In the spinal cord, results are more contradictory with some groups reporting

643 up to 20% loss of spinal motor neurons [11, 48], while we and others could not confirm this

644 [20]. This could be due to the small number of mice from which we could obtain spinal cord

645 tissue, which is one of the limitations of this study.

646 In human cases, we detected an average of 32.8% neurons cleared of nuclear TDP-43 in ALS

647 cases using an antibody directed against the C-terminal part of TDP-43, with control cases

648 showing an average of 13.18% neurons negative for nuclear TDP-43. Our human control cohort

649 showed relatively high basal levels of TDP-43 nuclear depletion, especially when compared to

650 6 and 16 months old wild-type mice. Since previous studies [28, 33] described this phenomenon

651 but, to our knowledge, did not provide quantitative data, it is unclear whether the detection of

652 TDP-43 nuclear clearance in control cases is a physiological finding, or whether it is due to

653 technical reasons (antibody sensitivity in formalin-fixed tissue) or autolysis during the *post-*

654 *mortem* interval. Importantly, it was shown that cellular stress can induce the depletion of TDP-

655 43 from the nucleus [38], which also occurs in normal aging and during the agonal phase before

656 death, possibly explaining the relatively high baseline levels of TDP-43 nuclear clearance in

657 the human control cohort. In contrast, mice were euthanized under anesthesia and brains were

658 immediately harvested, resulting in less cellular stress and therefore possibly lower levels of

659 baseline TDP-43 nuclear clearance. More studies on TDP-43 nuclear clearance including other

660 TDP-43 antibodies will be needed to clarify its biology.

661 Contrary to cleaved GSDMD, we did not observe an increase of caspase-1-positive microglia

662 in ALS versus control precentral gray and white matter using immunohistochemical methods

663 (Table 4). It is likely that mainly physiological inactive pro-caspase-1 is detected by

664 immunohistochemistry, which might mask the detection of increased levels of the active p20

665 fragment as observed by western blot (Table 4). It seems that full length pro-caspase-1 is

666 endogenously present in microglia, as control cases also show basal caspase-1 levels.

667 Furthermore, the abundance of caspase-1-positive microglia is five-fold higher compared to

668 cleaved GSDMD-positive microglia in human cases, indicating a physiological expression of

669 pro-caspase-1 in microglia. Using biochemical methods, we however observed an increased

670 expression of both pro-caspase-1 as well as the p20 active fragment in human ALS brain and

671 spinal cord (Table 4), probably reflecting a higher cellular expression without an increase in the

672 number of caspase-1 expressing microglial cells. Therefore, it is likely that in ALS microglia

673 upscale their expression of pro-caspase-1, and that following NLRP3 inflammasome activation

674 the p20 fragment is produced, as reflected by our western blot data (Table 4). We detected

675 similar results in mice, as symptomatic TDP-43^{A315T} did not show an increase in caspase-1-

676 positive microglia. However, an age-dependent effect was noted as 16 months old wild-type

677 and TDP-43^{A315T} transgenic mice presented with a higher abundance of caspase-1-positive glia

678 compared to their 6 months old counterparts. This age-dependent increase of caspase-1

679 expression was recently described in mice and humans and referred to as 'inflammaging',

680 reflecting the increased expression of inflammatory proteins during the aging process [30].

681 Additionally, the *post-mortem* interval and other comorbid neurological and agonal conditions

682 may influence the inflammatory status in the human brain and spinal cord, likely explaining the

683 higher baseline levels of caspase-1 and cleaved GSDMD-positive microglia in human *post-*

684 *mortem* tissue compared to wild-type and TDP-43^{A315T} transgenic mice, where these parameters

685 are better controlled. A limitation of this study is that we could not assess caspase-1 full length

686 and p20 fragment levels biochemically by western blot in mouse brain and spinal cord due to

687 unavailability of frozen tissue.

688 Our biochemical analysis in CNS lysates showed an increased expression of active IL-18 in

689 ALS motor cortex and spinal cord compared to control cases, indicative of an activated

690 pyroptosis pathway. Elevated serum IL-18 levels have previously also been demonstrated in

691   sporadic ALS patients [21]. Other groups reported elevated caspase-1, NLRP3 and IL-18 levels

692   in ALS brain tissue [22, 23], which is in line with our results for caspase-1, p20 and IL-18 in

693   the motor cortex and spinal cord. Increased NLRP3 mRNA levels were also detected in blood

694   and in *post-mortem* tissue of ALS patients [1, 32]. Unfortunately, antibodies against NLRP3

695   and IL-1β could not detect the respective proteins in *post-mortem* brain and spinal cord lysates

696   by western blot in our hands, which is a limitation of this study. Regarding the active fragment

697   of GSDMD, we showed for the first time an increased expression of cleaved GSDMD in ALS

698   versus control cases, which was significant in the spinal cord. It is possible that in the motor

699   cortex, baseline expression of cleaved GSDMD in neurons in both control and ALS cases, as

700   observed by IHC, masks the increased cleaved GSDMD expression in microglial cells on

701   western blot.

702   In the CNS, PRRs are thought to mainly be expressed on microglia and astrocytes [50]. Both

703   cell types also are assumed to be able to express NLRP3, however, for neurons this is still

704   debated [39]. In this study, we observed expression of the full NLRP3 inflammasome (i.e.

705   NLRP3, ASC and caspase-1) as well as the pyroptosis effector-related proteins cleaved

706   GSDMD and IL-18 in microglia. NLRP3 and cleaved GSDMD expression were additionally

707   detected in neurons and astrocytes, although to a lesser extent. ASC was exclusively detected

708   in microglia, while caspase-1 was also occasionally faintly stained in astrocytes. IL-18 was

709   absent in astrocytes, with some neurons faintly positive. Oligodendrocytes were negative for all

710   abovementioned markers. Our results underline the importance of microglia in inflammasome-

711   mediated pyroptosis in ALS, and are in line with several *in vitro* studies, showing that microglia

712   express the full NLRP3 inflammasome and produce active IL-1β and IL-18 [10, 25, 53].

713   Bellezza and colleagues also demonstrated expression of the NLRP3 inflammasome in

714   SOD1^{G93A} mouse microglial cells [2], although others found increased microglial caspase-1 and

715   ASC expression in the same mouse model, but not NLRP3 [29]. In contrast, another group

716   postulated mainly astrocytes, but also neurons to express ASC and NLRP3, with microglia only

717   positive for ASC in SOD1^{G93A} mice [8, 22]. A recent study, however, detected NLRP3

718   expression both in microglia and astrocytes of SOD1^{G93A} mice [10], similar to our results.

719   Overall, evidence points towards microglia as the main cell type responsible for pyroptosis

720   activation in ALS, although we cannot fully exclude that astrocytes and possibly neurons also

721   contribute to NLRP3 inflammasome-mediated cytotoxicity.

722   In conclusion, our findings point towards microglial NLRP3 inflammasome-mediated

723   pyroptosis as an important player in ALS pathophysiology and neurodegeneration, with cleaved

724   GSDMD as a useful marker for pyroptosis activation in the ALS precentral white matter.

725   Investigation of the pathological triggers and the effects of inhibition of this pathway *in vitro*

726   and *in vivo* will aid in the development of novel therapeutic strategies counteracting motor

727   neuron degeneration in ALS.

728

729

Author contributions

EVS: study design and coordination, immunohistochemistry, immunofluorescence, protein extraction, western blotting, microscopic assessments, neuropathology, statistical analysis, manuscript drafting and preparation. SO: mouse immunohistochemistry, immunofluorescence, critical review of the manuscript. SM: immunohistochemistry, western blotting, critical review of the manuscript. ST: design of mouse study, mouse genotyping, critical review of the manuscript. AR: design of mouse study, mouse breeding, mouse sacrificing and tissue collection, critical review of the manuscript. OO: human immunohistochemistry, western blotting, critical review of the manuscript. JW and ACL: clinical neurology, critical review of the manuscript. PVD: clinical neurology, study design, critical review of the manuscript. LVDB: study design, critical review of the manuscript. DRT: study design and supervision, neuropathology and manuscript preparation. All authors read and approved the final manuscript.

Disclosures/Conflicts of Interest

ACL serves on the Advisory Board of Roche Pharma (Basel, Switzerland) and Biogen (Cambridge, MA, US), and on the data and safety monitoring board of Zeneus pharma (Bray, UK). ACL received consulting fees from AB Science (Paris, France), Desitin (Buckinghamshire, UK), Novartis (Basel, Switzerland) and Teva (Jerusalum, Israel). PVD participated in advisory board meetings of Biogen (Cambridge, MA, US), Cytokinetics (San Francisco, CA, US), Ferrer (Barcelona, Spain), UCB (Brussels, Belgium), Argenx (Ghent, Belgium), Muna Therapeutics (Copenhagen, Denmark), Alector (San Francisco, CA, US), Augustine Therapeutics (Leuven, Belgium), Alexion Therapeutics (Boston, MA, US) and QurAlis (Cambridge, MA, US). LVDB received speaker honorary from UCB (Brussels, Belgium) and Grünenthal (Aachen, Germany), and is head of the Scientific Advisory Board of Augustine Therapeutics (Leuven, Belgium) and is part of the Investment Advisory Board of

763

764

Figures and Tables

Figure 1. Expression of inflammasome components and pyroptosis effector-related proteins in ALS precentral white matter microglia. Immunohistochemical and immunofluorescence detection of inflammasome components NLRP3 (a-e), ASC (f-j) and caspase-1 (k-o), as well as pyroptosis effector-related proteins cleaved GSDMD (p-t) and IL-18 (u-y) in representative ALS precentral white matter. Arrowheads indicate microglial cells positive for the respective markers. Scale bars represent 50 μm.

Figure 2. Increased expression of cleaved GSDMD in ALS microglial cells in the precentral white matter. (a, b) Graphs representing the number of microglia per mm² positive for caspase-1 (a) and cleaved GSDMD (b) in layer V of the motor cortex of control and ALS cases. **(c, d)** Graphs representing the number of microglia per mm² positive for caspase-1 (c) and cleaved GSDMD (d) in the precentral white matter of control and ALS cases. Binary logistic regression corrected for age and sex was used for statistical analysis. * $p < 0.05$.

Figure 3. Motor cortex layer V neuronal density and pTDP-43 pathology. (a) Graph representing the neuronal density per mm² in layer V of the motor cortex of control and ALS cases. **(b)** Graph representing the percentage of pTDP-43 affected neurons in the motor cortex of control and ALS cases. **(c)** Graph representing the percentage of neurons with TDP-43 cleared from the nucleus in layer V of the motor cortex. Binary logistic regression corrected for age and sex or a Mann-Whitney test was used for statistical analysis. * $p < 0.05$.

Figure 4. Biochemical characterization of pyroptosis proteins in the ALS motor cortex. **(a)** Motor cortex tissue lysates from control (n = 7) and ALS (n = 8) on western blots probed with antibodies for caspase-1, cleaved GSDMD and IL-18, with GAPDH as loading control. **(b-e)** Quantifications of pyroptosis-related proteins relative to GAPDH. Statistical analyses were preformed using unpaired t-test or Mann-Whitney test. *** $p < 0.001$; **** $p < 0.0001$.

789 **Figure 5. Expression of caspase-1 and cleaved GSDMD in ALS and control spinal cord**

790 **pyramidal tract microglia. (a, b)** Graphs representing the number of microglia per mm²

791 positive for caspase-1 (a) and cleaved GSDMD (b) in the ventral pyramidal tracts of control

792 and ALS spinal cord. **(c, d)** Graphs representing the number of microglia per mm² positive for

793 caspase-1 (c) and cleaved GSDMD (d) in the lateral pyramidal tracts of control and ALS spinal

794 cord. Binary logistic regression corrected for age and sex was used for statistical analysis.

795 **Figure 6. Biochemical characterization of pyroptosis proteins in the ALS spinal cord. (a)**

796 Spinal cord tissue lysates from control (n = 8) and ALS (n = 7) on western blots probed with

797 antibodies for caspase-1, cleaved GSDMD and IL-18, with GAPDH as loading control. For IL-

798 18, the lower band is the correct molecular weight, as the upper band represents pro-IL-18. **(b-**

799 **e)** Quantifications of pyroptosis-related proteins relative to GAPDH. Statistical analyses were

800 preformed using unpaired t-test or Mann-Whitney test. * $p < 0.05$; ** $p < 0.01$; *** $p < 0.001$.

801 **Figure 7. Increased expression of GSDMD in motor cortex and spinal cord of symptomatic**

802 **TDP-43^{A315T} transgenic mice. (a)** Immunohistochemical representative image of caspase-1-

803 positive microglia (arrowheads) in the motor cortex of TDP-43^{A315T} transgenic mice. **(b)**

804 Immunohistochemical representative image of GSDMD-positive microglia (arrowheads) in the

805 motor cortex of TDP-43^{A315T} transgenic mice. Scale bars represent 50 µm. **(c,d)** Graphs

806 representing the number of caspase-1 (c) and GSDMD (d) positive microglia per mm² in the

807 motor cortex of the different mouse groups. **(e,f)** Graphs representing the number of caspase-1

808 (e) and GSDMD (f) positive microglia per mm² in the spinal cord of the different mouse groups.

809 WT 6m = 6 months old wild-type mice; WT 16m = 16 months old wild-type mice; TDP Tg 6m

810 = 6 months old TDP-43^{A315T} transgenic mice; TDP Tg 16m = 16 months old TDP-43^{A315T}

811 transgenic mice; TDP symp = symptomatic TDP^{A315T} transgenic mice. * $p < 0.05$; ** $p < 0.01$;

812 *** $p < 0.001$.

813

Table 1. Overview of the expression of inflammasome components and pyroptosis effector-related proteins in different cell types. +++ abundant strongly positive cells; (+++) abundant faintly positive cells; ++ some strongly positive cells; (++) some faintly positive cells; + few strongly positive cells; (+) few faintly positive cells.

	Neurons	Astrocytes	Microglia	Oligodendrocytes
NLRP3	(+)	+	+++	-
ASC	-	-	+++	-
Caspase-1	-	(+)	+++	-
Cleaved GSDMD	(++)	+	+++	-
IL-18	(+)	-	+++	-

Table 2. Correlation matrix for motor cortex layer V neuronal density and other parameters, corrected for age and sex. Matrix showing Pearson's correlation values and p-values for the association between motor cortex layer V neuronal density and other variables, including the number of caspase-1-positive microglia in the precentral white matter, the number of cleaved GSDMD-positive microglia in the precentral white matter, the percentage of pTDP-43 affected neurons in the motor cortex, and the percentage of neurons with TDP-43 nuclear clearance in layer V of the motor cortex. * $p < 0.05$; ** $p < 0.01$.

	Caspase-1 positive microglia	Cl GSDMD-positive microglia	% pTDP-43 affected neurons	Neuronal density	% TDP-43 clearance	n
Caspase-1 positive microglia	-					25
Cl GSDMD-postive microglia	r = 0.020; p = 0.921	-				25
% pTDP-43 affected neurons	r = 0.083; p = 0.682	r = -0.010; p = 0.960	-			25
Neuronal density motor cortex layer V	r = -0.343; p = 0.080	r = -0.431; p = 0.025*	r = -0.504; p = 0.007**	-		25
% TDP-43 clearance	r = 0.282; p = 0.163	r = 0.116; p = 0.572	r = 0.035; p = 0.865	r = -0.313; p = 0.119	-	24

Table 3. Correlation matrix for mouse motor cortex neuronal density and other parameters. Matrix showing Pearson's correlation values and p-values for the association between mouse motor cortex layer V neuronal density and other variables, including the number of caspase-1-positive microglia , the number of GSDMD-positive microglia, and the percentage of TDP-43 nuclear clearance. * $p < 0.05$; ** $p < 0.01$.

	Caspase-1-positive microglia	GSDMD-positive microglia	% TDP-43 clearance	Layer V neuronal density	n
Caspase-1-positive microglia	-				23
GSDMD-positive microglia	r = -0.075; p = 0.733	-			23
% TDP-43 clearance	r = -0.168; p = 0.442	r = 0.408; p = 0.053	-		23
Layer V neuronal density	r = -0.378; p = 0.075	r = -0.478; p = 0.021*	r = -0.692; p < 0.001**	-	23

Table 4. Overview for the comparison of IHC versus WB results for caspase-1 and cleaved GSDMD in the human and mouse motor cortex and spinal cord. In immunohistochemical stainings the number of cells expressing a given protein was assessed, whereas by western blot the general expression levels were determined. GM = gray matter; WM = white matter; IHC = immunohistochemistry; WB = western blot; ↑ = significant increase; ↗ = numerical trend towards increase; "=" = no noticeable difference; ↓ = significant decrease.

		CASPASE-1	
		IHC	WB
Human ALS	Motor cortex	WM = GM ↓	Pro-caspase-1 ↑ Caspase-1 p20 ↑
	Spinal cord	WM =	Pro-caspase-1 ↑ Caspase-1 p20 ↑
Mouse TDP-43 A315T	Motor cortex	=	
	Spinal cord	=	

		CLEAVED GSDMD	
		IHC	WB
Human ALS	Motor cortex	WM ↑ GM =	cl GSDMD ↗
	Spinal cord	WM ↗	cl GSDMD ↑
Mouse TDP-43 A315T	Motor cortex	↑	
	Spinal cord	↑	

References

1. Banerjee P, Elliott E, Rifai OM, O'Shaughnessy J, McDade K, Abrahams S, Chandran S, Smith C, Gregory JM (2022) NLRP3 inflammasome as a key molecular target underlying cognitive resilience in amyotrophic lateral sclerosis. J Pathol 256:262–268. doi: 10.1002/path.5846

2. Bellezza I, Grottelli S, Costanzi E, Scarpelli P, Pigna E, Morozzi G, Mezzasoma L, Peirce MJ, Moresi V, Adamo S, Minelli A (2018) Peroxynitrite Activates the NLRP3 Inflammasome Cascade in SOD1(G93A) Mouse Model of Amyotrophic Lateral Sclerosis. Mol Neurobiol 55:2350–2361. doi: 10.1007/s12035-017-0502-x

3. Braak H, Alafuzoff I, Arzberger T, Kretzschmar H, Del Tredici K (2006) Staging of Alzheimer disease-associated neurofibrillary pathology using paraffin sections and immunocytochemistry. Acta Neuropathol 112:389–404. doi: 10.1007/s00401-006-0127-z

4. Brooks BR, Miller RG, Swash M, Munsat TL (2000) El Escorial revisited: revised criteria for the diagnosis of amyotrophic lateral sclerosis. Amyotroph Lateral Scler 1:293–299. doi: 10.1080/146608200300079536

5. de Carvalho M, Dengler R, Eisen A, England JD, Kaji R, Kimura J, Mills K, Mitsumoto H, Nodera H, Shefner J, Swash M (2008) Electrodiagnostic criteria for diagnosis of ALS. Clin Neurophysiol 119:497–503. doi: 10.1016/j.clinph.2007.09.143

6. De Carvalho M, Swash M (2009) Awaji diagnostic algorithm increases sensitivity of El Escorial criteria for ALS diagnosis. Amyotroph Lateral Scler 10:53–57. doi: 10.1080/17482960802521126

7. Debray S, Race V, Crabbé V, Herdewyn S, Matthijs G, Goris A, Dubois B, Thijs V, Robberecht W, Van Damme P (2013) Frequency of C9Orf72 repeat expansions in amyotrophic lateral sclerosis: a Belgian cohort study. Neurobiol Aging 34:2890.e7-2890.e12. doi: 10.1016/j.neurobiolaging.2013.06.009

8. Debye B, Schmülling L, Zhou L, Rune G, Beyer C, Johann S (2018) Neurodegeneration and NLRP3 inflammasome expression in the anterior thalamus of SOD1(G93A) ALS mice. Brain Pathol 28:14–27. doi: 10.1111/bpa.12467

9. Denes A, Brough D (2012) Caspase-1: is IL-1 just the tip of the ICEberg? Cell Death Dis 3:e338. doi: 10.1038/cddis.2012.86

10. Deora V, Lee JD, Albornoz EA, Mcalary L, Jagaraj CJ, Robertson AAB, Atkin JD, Cooper MA, Schroder K, Yerbury JJ, Gordon R, Woodruff TM (2019) The microglial NLRP3 inflammasome is activated by amyotrophic lateral sclerosis proteins. Glia 68:407–421. doi: 10.1002/glia.23728

11. Espejo-Porras F, Piscitelli F, Verde R, Ramos JA, Di Marzo V, de Lago E, Fernández-Ruiz J (2015) Changes in the endocannabinoid signaling system in CNS structures of TDP-43 transgenic mice: relevance for a neuroprotective therapy in TDP-43-related disorders. J Neuroimmune Pharmacol 10:233–244. doi: 10.1007/s11481-015-9602-4

12. Frank D, Vince JE (2019) Pyroptosis versus necroptosis: similarities, differences, and crosstalk. Cell Death Differ 26:99–114. doi: 10.1038/s41418-018-0212-6

13. Gao J, Wang L, Huntley ML, Perry G, Wang X (2018) Pathomechanisms of TDP-43 in neurodegeneration. J Neurochem 146:7–20. doi: 10.1111/jnc.14327

14. Gorno-Tempini ML, Hillis AE, Weintraub S, Kertesz A, Mendez M, Cappa SF, Ogar JM, Rohrer JD, Black S, Boeve BF, Manes F, Dronkers NF, Vandenberghe R, Rascovsky K, Patterson K, Miller BL, Knopman DS, Hodges JR, Mesulam MM, Grossman M (2011) Classification of primary progressive aphasia and its variants. Neurology 76:1006–1014. doi:

891   10.1212/WNL.0b013e31821103e6

892 15. Guan Y, Han F (2020) Key Mechanisms and Potential Targets of the NLRP3 Inflammasome in
893   Neurodegenerative Diseases. Front Integr Neurosci 14:37. doi: 10.3389/fnint.2020.00037

894 16. Gugliandolo A, Giacoppo S, Bramanti P, Mazzon E (2018) NLRP3 Inflammasome Activation in
895   a Transgenic Amyotrophic Lateral Sclerosis Model. Inflammation 41:93–103. doi:
896   10.1007/s10753-017-0667-5

897 17. Hardiman O, Al-Chalabi A, Chio A, Corr EM, Logroscino G, Robberecht W, Shaw PJ, Simmons
898   Z, Van Den Berg LH (2017) Amyotrophic lateral sclerosis. Nat Rev Dis Prim 3:17071. doi:
899   10.1038/nrdp.2017.71

900 18. Hatzipetros T, Bogdanik LP, Tassinari VR, Kidd JD, Moreno AJ, Davis C, Osborne M, Austin
901   A, Vieira FG, Lutz C, Perrin S (2014) C57BL/6J congenic Prp-TDP43A315T mice develop
902   progressive neurodegeneration in the myenteric plexus of the colon without exhibiting key
903   features of ALS. Brain Res 1584:59–72. doi: 10.1016/j.brainres.2013.10.013

904 19. Heneka MT, Kummer MP, Stutz A, Delekate A, Saecker A, Griep A, Axt D, Remus A, Tzeng
905   T, Gelpi E, Halle A, Korte M, Latz E, Golenbock D (2013) NRLP3 is activated in Alzheimer's
906   disease and contributes to pathology in APP/PS1 mice. Nature 493:674–678. doi:
907   10.1038/nature11729.NLRP3

908 20. Herdewyn S, Cirillo C, Van Den Bosch L, Robberecht W, Vanden Berghe P, Van Damme P
909   (2014) Prevention of intestinal obstruction reveals progressive neurodegeneration in mutant
910   TDP-43 (A315T) mice. Mol Neurodegener 9:24. doi: 10.1186/1750-1326-9-24

911 21. Italiani P, Carlesi C, Giungato P, Puxeddu I, Borroni B, Bossù P, Migliorini P, Siciliano G,
912   Boraschi D (2014) Evaluating the levels of interleukin-1 family cytokines in sporadic
913   amyotrophic lateral sclerosis. J Neuroinflammation 11:94. doi: 10.1186/1742-2094-11-94

914 22. Johann S, Heitzer M, Kanagaratnam M, Goswami A, Rizo T, Weis J, Troost D, Beyer C (2015)
915   NLRP3 inflammasome is expressed by astrocytes in the SOD1 mouse model of ALS and in
916   human sporadic ALS patients. Glia 63:2260–2273. doi: 10.1002/glia.22891

917 23. Kadhim H, Deltenre P, Martin JJ, Sébire G (2016) In-situ expression of Interleukin-18 and
918   associated mediators in the human brain of sALS patients: Hypothesis for a role for immune-
919   inflammatory mechanisms. Med Hypotheses 86:14–17. doi: 10.1016/j.mehy.2015.11.022

920 24. Koper MJ, Van Schoor E, Ospitalieri S, Vandenberghe R, Vandenbulcke M, Von Arnim CAF,
921   Tousseyn T, Balusu S, De Strooper B, Thal DR (2019) Necrosome complex detected in
922   granulovacuolar degeneration is associated with neuronal loss in Alzheimer's disease. Acta
923   Neuropathol 139:463–484. doi: 10.1007/s00401-019-02103-y

924 25. Leal-lasarte M, Franco JM, Labrador-garrido A, Pozo D (2017) Extracellular TDP-43 aggregates
925   target MAPK/MAK/MRK overlapping kinase (MOK) and trigger caspase-3 / IL-18 signaling in
926   microglia. FASEB 7:2797–2816. doi: 10.1096/fj.201601163R

927 26. Lee J, Hamanaka G, Lo EH, Arai K (2019) Heterogeneity of microglia and their differential roles
928   in white matter pathology. CNS Neurosci Ther 25:1290–1298. doi: 10.1111/cns.13266

929 27. Lee J, Hyeon SJ, Im H, Ryu H, Kim Y, Ryu H (2016) Astrocytes and Microglia as Non-cell
930   Autonomous Players in the Pathogenesis of ALS. Exp Neurobiol 25:233. doi:
931   10.5607/en.2016.25.5.233

932 28. Mackenzie IRA, Bigio EH, Ince PG, Geser F, Neumann M, Cairns NJ, Kwong LK, Forman MS,
933   Ravits J, Stewart H, Eisen A, Mcclusky L, Kretzschmar HA, Monoranu CM, Highley JR, Kirby
934   J, Siddique T, Shaw PJ, Lee VM, Trojanowski JQ (2007) Pathological TDP-43 Distinguishes
935   Sporadic Amyotrophic Lateral Sclerosis from Amyotrophic Lateral Sclerosis with SOD1
936   Mutations. Ann Neurol 61:427–434. doi: 10.1002/ana.21147

937   29.   Meissner F, Molawi K, Zychlinsky A (2010) Mutant superoxide dismutase 1-induced IL-1beta
938   accelerates ALS pathogenesis. PNAS 107:13046–13050. doi: 10.1073/pnas.1002396107

939   30.   Mejias NH, Martinez CC, Stephens ME, De Rivero Vaccari JP (2018) Contribution of the
940   inflammasome to inflammaging. J Inflamm 15:23. doi: 10.1186/s12950-018-0198-3

941   31.   Mirra SS, Heyman A, McKeel DW, Sumi SM, Crain BJ, Brownlee LM, Vogel FS, Hughes JP,
942   Van Belle G, Berg L (1991) The Consortium to Establish a Registry for Alzheimer's Disease
943   (CERAD): II. Standardization of the neuropathologic assessment of Alzheimer's disease.
944   Neurology 41:479–486

945   32.   Moreno-García L, Miana-Mena FJ, Moreno-Martínez L, de la Torre M, Lunetta C, Tarlarini C,
946   Zaragoza P, Calvo AC, Osta R (2021) Inflammasome in ALS Skeletal Muscle: NLRP3 as a
947   Potential Biomarker. Int J Mol Sci 22:2523. doi: 10.3390/ijms22052523

948   33.   Neumann M, Sampathu DM, Kwong LK, Truax AC, Micsenyi MC, Chou TT, Bruce J, Schuck
949   T, Grossman M, Clark CM, McCluskey LF, Miller BL, Masliah E, Mackenzie IR, Feldman H,
950   Feiden W, Kretzschmar HA, Trojanowski JQ, Lee VM-Y (2006) Ubiquitinated TDP-43 in
951   Frontotemporal Lobar Degeneration and Amyotrophic Lateral Sclerosis. Science (80-) 314:130–
952   133. doi: 10.1126/science.1134108

953   34.   Philips T, Robberecht W (2011) Neuroinflammation in amyotrophic lateral sclerosis: role of glial
954   activation in motor neuron disease. Lancet Neurol 10:253–263

955   35.   Rascovsky K, Hodges JR, Knopman D, Mendez MF, Kramer JH, Neuhaus J, Van Swieten JC,
956   Seelaar H, Dopper EGP, Onyike CU, Hillis AE, Josephs KA, Boeve BF, Kertesz A, Seeley WW,
957   Rankin KP, Johnson JK, Gorno-Tempini ML, Rosen H, Prioleau-Latham CE, Lee A, Kipps CM,
958   Lillo P, Piguet O, Rohrer JD, Rossor MN, Warren JD, Fox NC, Galasko D, Salmon DP, Black
959   SE, Mesulam M, Weintraub S, Dickerson BC, Diehl-Schmid J, Pasquier F, Deramecourt V,
960   Lebert F, Pijnenburg Y, Chow TW, Manes F, Grafman J, Cappa SF, Freedman M, Grossman M,
961   Miller BL (2011) Sensitivity of revised diagnostic criteria for the behavioural variant of
962   frontotemporal dementia. Brain 134:2456–2477. doi: 10.1093/brain/awr179

963   36.   Renton AE, Chio A, Traynor BJ (2014) State of play in amyotrophic lateral sclerosis. Nat
964   Neurosci 17:17–23. doi: 10.1038/nn.3584.

965   37.   Rosenbohm A, Peter RS, Erhardt S, Lulé D, Rothenbacher D, Ludolph AC, Nagel G, The ALS
966   Registry Study Group, Andres F, Arnold G, Asshauer I, Baezner H, Baier H, Beattie J, Becker
967   T, Behne F, Bengel D, Boertlein A, Bracknies V, Broer R, Burkhard A, Connemann B,
968   Dempewolf S, Dettmers C, Dieterich M, Etzersdorfer E, Freund W, Gersner T, Gold HJ, Hacke
969   W, Hamann G, Hecht M, Heimbach B, Hemmer B, Hendrich C, Herting B, Huber R, Huber-
970   Hartmann K, Hülser PJ, Jüttler E, Kammerer-Ciernioch J, Kaspar A, Kern R, Kimmig H, Klebe
971   S, Kloetzsch C, Klopstock T, Kohler A, Kuethmann A, Lewis D, Lichy C, Lindner A, Mäurer
972   M, Maier-Janson W, Metrikat J, Meudt O, Meyer A, Müller vom Hagen J, Naegele A, Naumann
973   M, Neher KD, Neuhaus O, Neusch C, Niehaus L, Opherk C, Raape J, Ratzka P, Rettenmayr C,
974   Riepe MW, Rothmeier J, Sabolek M, Schabet M, Schell C, Schlipf T, Schmauss M, Schoels L,
975   Schuetz K, Schweigert B, Sommer N, Sperber W, Steber C, Steber R, Stroick M, Synofzik M,
976   Trottenberg T, Tumani H, Wahl C, Weber F, Weiler M, Weiller C, Wessig C, Winkler A (2017)
977   Epidemiology of amyotrophic lateral sclerosis in Southern Germany. J Neurol 264:749–757. doi:
978   10.1007/s00415-017-8413-3

979   38.   Scotter EL, Chen HJ, Shaw CE (2015) TDP-43 Proteinopathy and ALS: Insights into Disease
980   Mechanisms and Therapeutic Targets. Neurotherapeutics 12:352–363. doi: 10.1007/s13311-015-
981   0338-x

982   39.   Song L, Pei L, Yao S, Wu Y, Shang Y (2017) NLRP3 Inflammasome in Neurological Diseases,
983   from Functions to Therapies. Front Cell Neurosci 11:63. doi: 10.3389/fncel.2017.00063

984   40.   Swinnen B, Robberecht W (2014) The phenotypic variability of amyotrophic lateral sclerosis.

985   Nat Rev Neurol 10:661–670. doi: 10.1038/nrneurol.2014.184

986   41.   Taylor JP, Brown RH, Cleveland DW (2016) Decoding ALS: From Genes to Mechanism. Nature
987   539:197–206. doi: 10.1126/science.1249098

988   42.   Thal DR, Rüb U, Schultz C, Sassin I, Ghebremedhin E, Del Tredici K, Braak E, Braak H (2000)
989   Sequence of Aβ-protein deposition in the human medial temporal lobe. J Neuropathol Exp
990   Neurol 59:733–748. doi: 10.1093/jnen/59.8.733

991   43.   Van Damme P, Robberecht W, Van Den Bosch L (2017) Modelling amyotrophic lateral
992   sclerosis: progress and possibilities. Dis Model Mech 10:537–549. doi: 10.1242/dmm.029058

993   44.   Van der Poel M, Ulas T, Mizee MR, Hsiao C, Miedema SSM, Schuurman KG, Helder B, Tas
994   SW, Schultze JL, Hamann J, Huitinga I (2019) Transcriptional profiling of human microglia
995   reveals grey-white matter heterogeneity and multiple sclerosis-associated changes. Nat Commun
996   10:1139. doi: 10.1038/s41467-019-08976-7

997   45.   Van Schoor E, Koper MJ, Ospitalieri S, Dedeene L, Tomé SO, Vandenberghe R, Brenner D,
998   Otto M, Weishaupt J, Ludolph AC, Van Damme P, Van Den Bosch L, Thal DR (2020)
999   Necrosome-positive granulovacuolar degeneration is associated with TDP-43 pathological
1000   lesions in the hippocampus of ALS/FTLD cases. Neuropathol Appl Neurobiol 47:328–345. doi:
1001   10.1111/nan.12668

1002   46.   Vande Walle L, Lamkanfi M (2016) Pyroptosis. Curr Biol 26:R568–R572. doi:
1003   10.1016/j.cub.2016.02.019

1004   47.   Wang X, Chi J, Huang D, Ding L, Zhao X, Jiang L, Yu Y, Gao F (2020) α-synuclein promotes
1005   progression of Parkinson's disease by upregulating autophagy signaling pathway to activate
1006   NLRP3 inflammasome. Exp Ther Med 19:931–938. doi: 10.3892/etm.2019.8297

1007   48.   Wegorzewska I, Bell S, Cairns NJ, Miller TM, Baloh RH (2009) TDP-43 mutant transgenic mice
1008   develop features of ALS and frontotemporal lobar degeneration. PNAS 106:18809–18814. doi:
1009   10.1073/pnas.0908767106

1010   49.   Wijesekera LC, Leigh PN (2009) Amyotrophic lateral sclerosis. Orphanet J Rare Dis 4:3. doi:
1011   10.1186/1750-1172-4-3

1012   50.   Xie Z, Zhao G (2014) Pyroptosis and neurological diseases. Neuroimmunol Neuroinflammation
1013   1:60–65. doi: 10.4103/2347-8659.139716

1014   51.   Zhang W, Zhang L, Liang B, Schroeder D, Zhang Z, Cox GA, Li Y, Lin D (2016) Hyperactive
1015   somatostatin interneurons contribute to excitotoxicity in neurodegenerative disorders. Nat
1016   Neurosci 19:557–559. doi: 10.1038/nn.4257

1017   52.   Zhang X, Wang R, Hu D, Sun X, Fujioka H, Lundberg K, Chan ER, Wang Q, Xu R, Flanagan
1018   ME, Pieper AA, Qi X (2020) Oligodendroglial glycolytic stress triggers inflammasome
1019   activation and neuropathology in Alzheimer's disease. Sci Adv 6:eabb8680. doi:
1020   10.1126/sciadv.abb8680

1021   53.   Zhao W, Beers DR, Bell S, Wang J, Wen S, Baloh RH, Appel SH (2015) TDP-43 activates
1022   microglia through NF-κB and NLRP3 inflammasome. Exp Neurol 273:24–35. doi:
1023   10.1016/j.expneurol.2015.07.019

1024   54.   Zhou K, Shi L, Wang Y, Chen S, Zhang J (2016) Recent Advances of the NLRP3 Inflammasome
1025   in Central Nervous System Disorders. J Immunol Res 2016:9238290. doi:
1026   10.1155/2016/9238290

1027   55.   Zhu J, Cynader MS, Jia W (2015) TDP-43 Inhibits NF-κB Activity by Blocking p65 Nuclear
1028   Translocation. PLoS One 10:e0142296. doi: 10.1371/journal.pone.0142296

1029

Figure 1. Expression of inflammasome components and pyroptosis effector proteins in ALS precentral white matter microglia
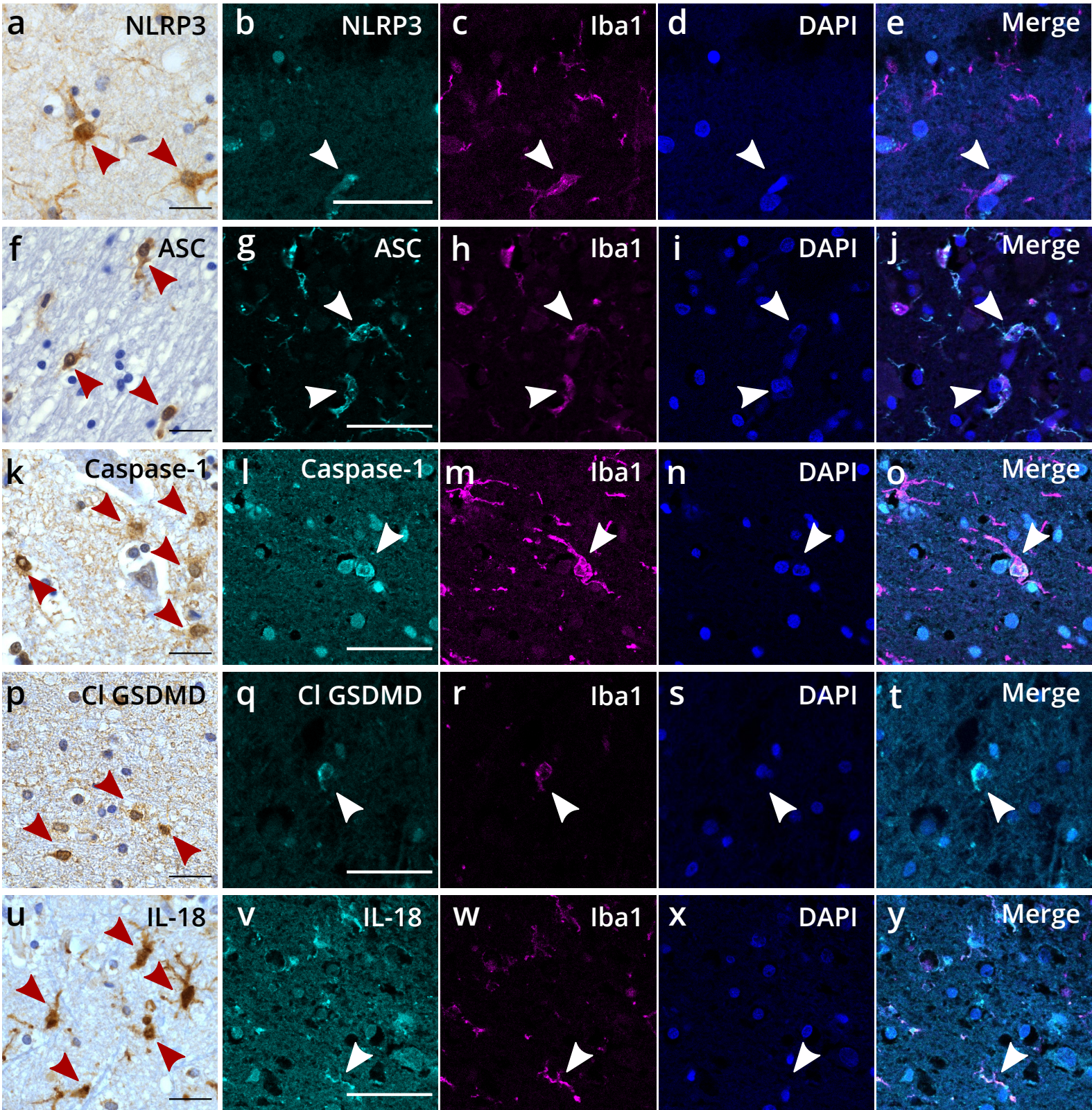
Figure 2. Increased expression of cleaved GSDMD in ALS microglia cells in the precentral white matter

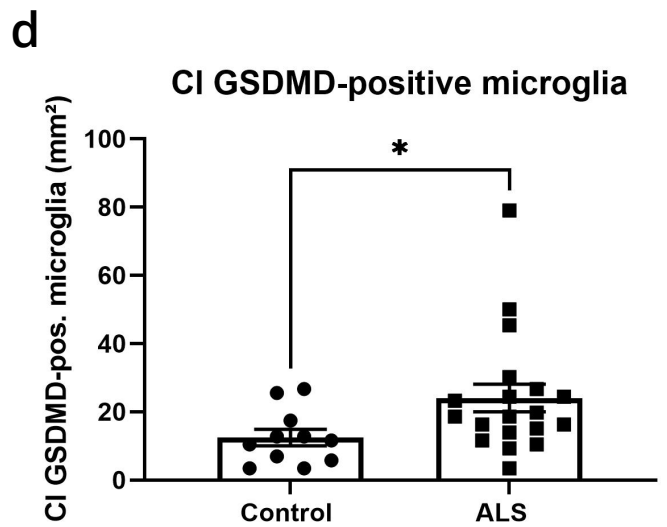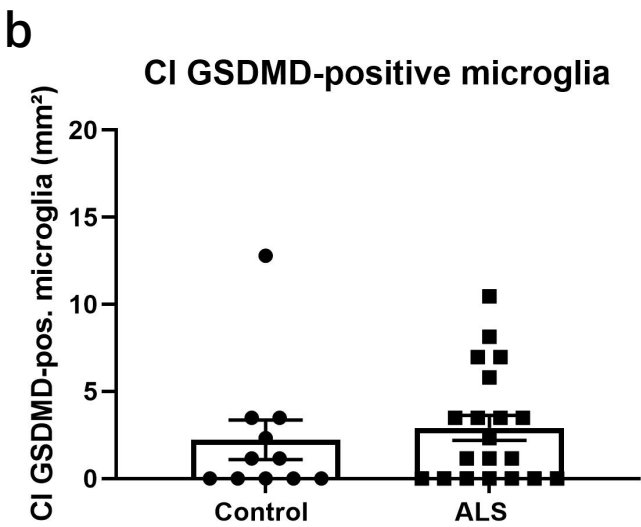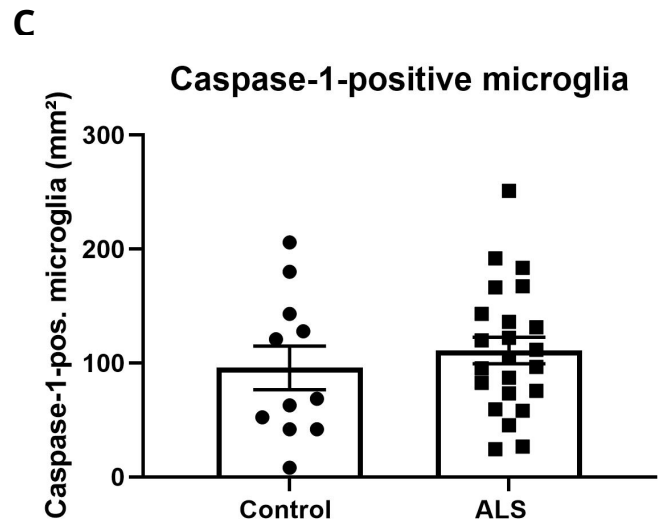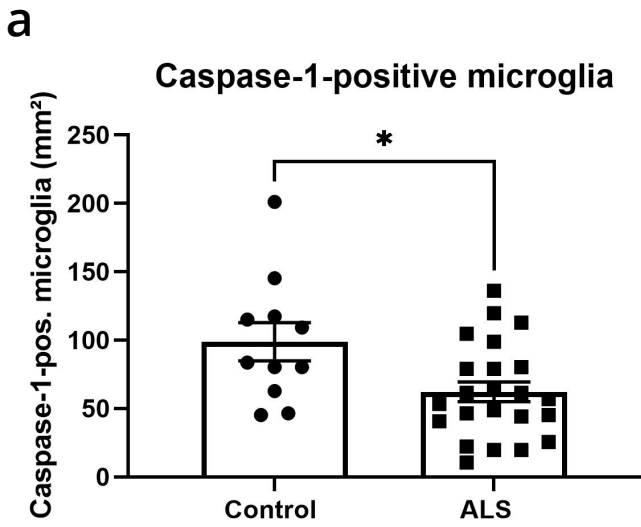# Figure 3. Motor cortex pTDP-43 pathology and layer V neuronal density.

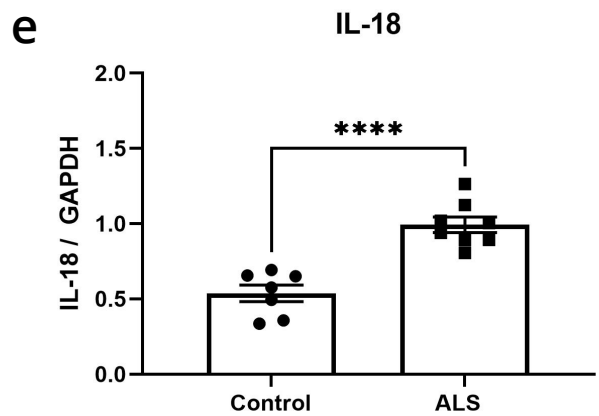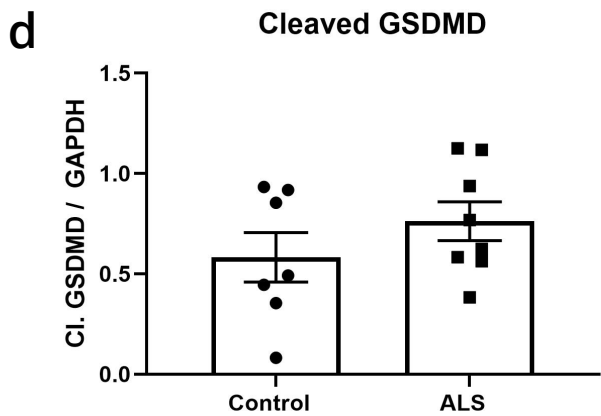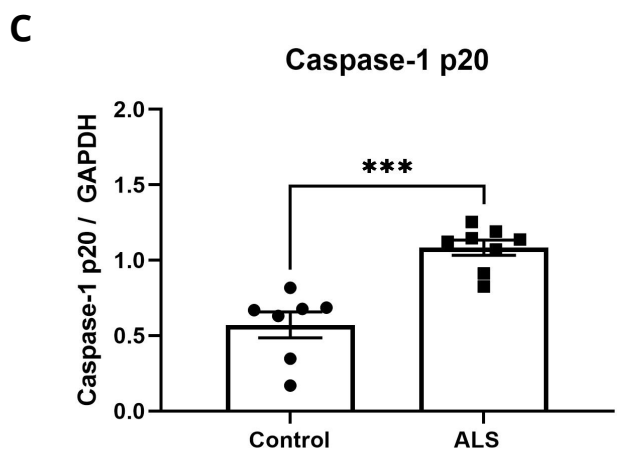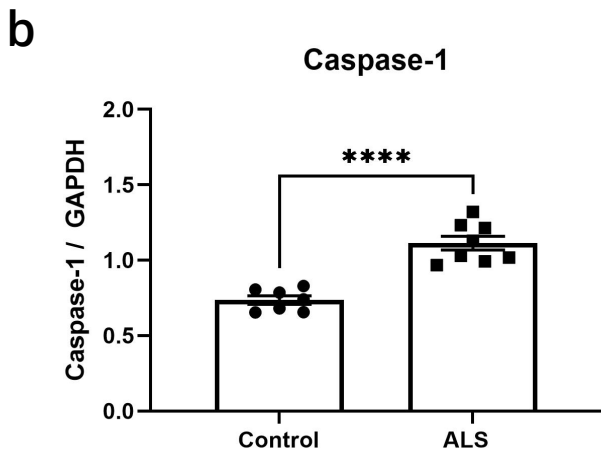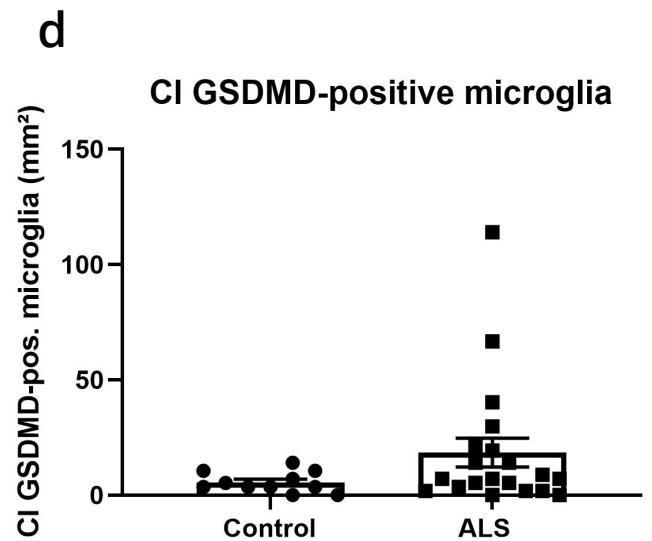Figure 4. Biochemical characterization of pyroptosis-proteins in the ALS motor cortex.
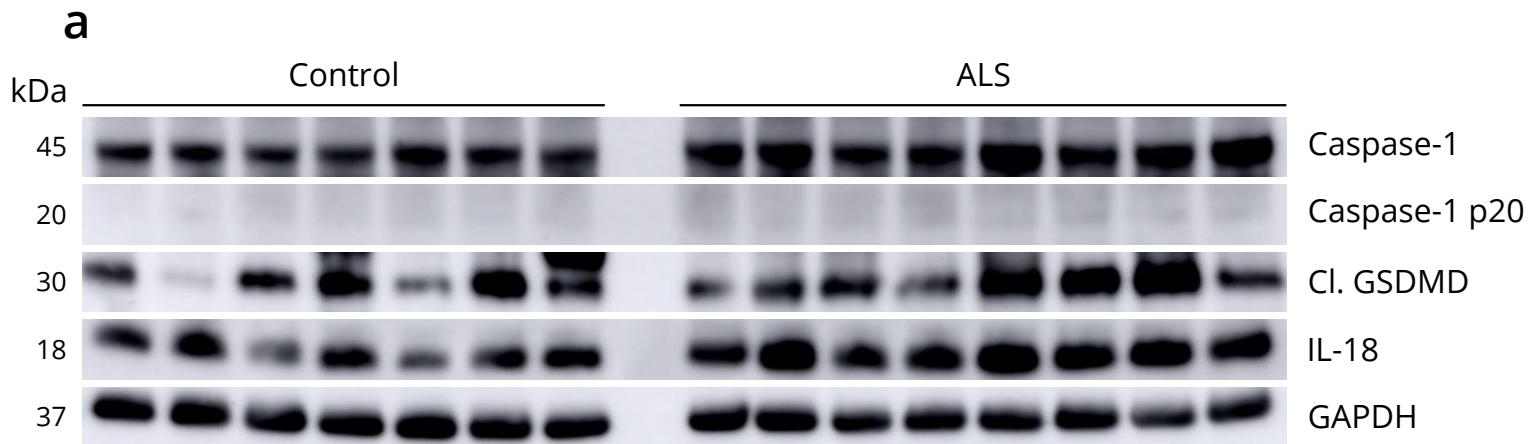
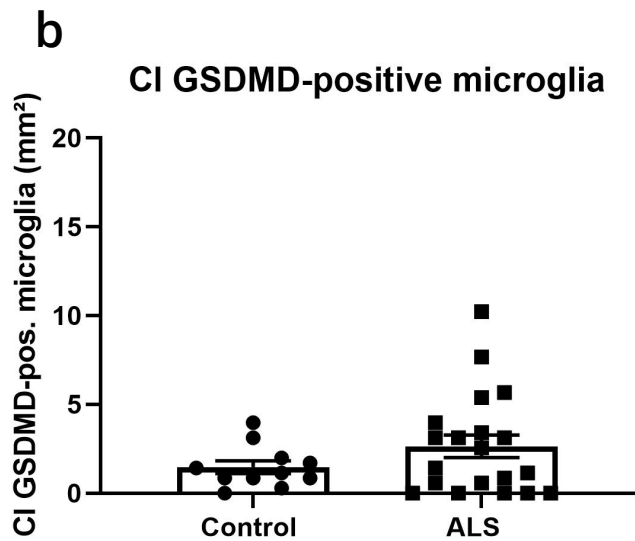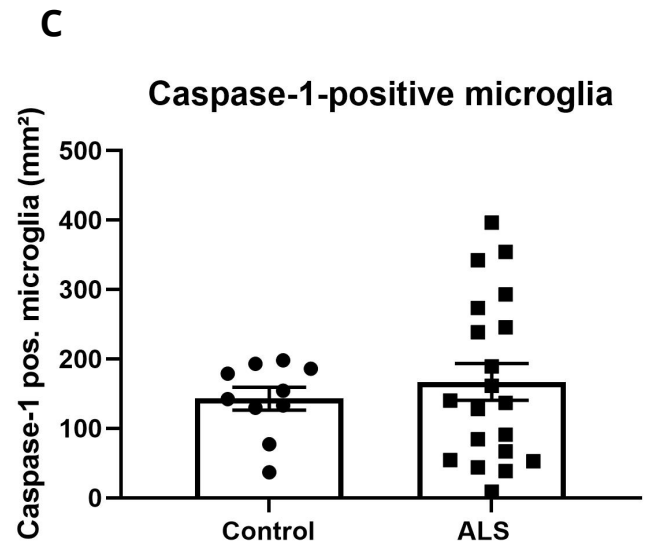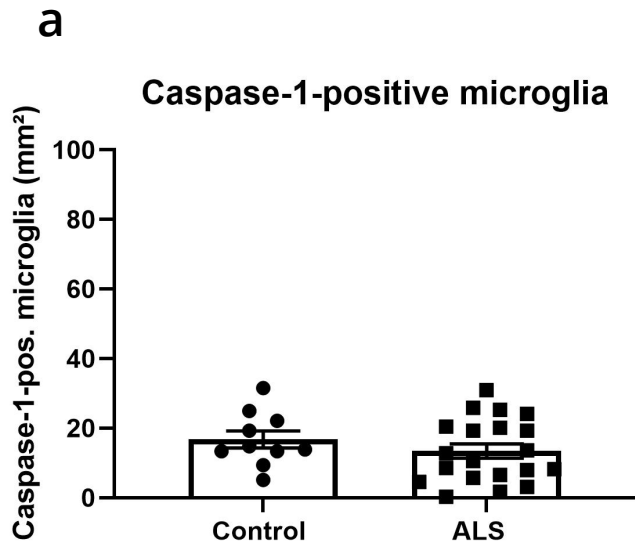# Figure 5. Expression of caspase-1 and cleaved GSDMD in ALS and control spinal cord pyramidal tract microglia.

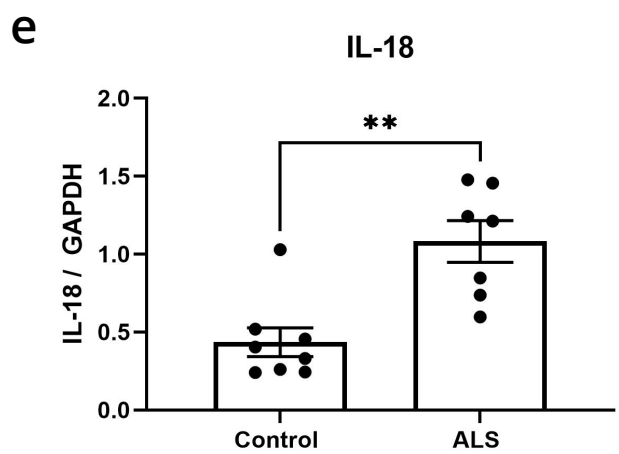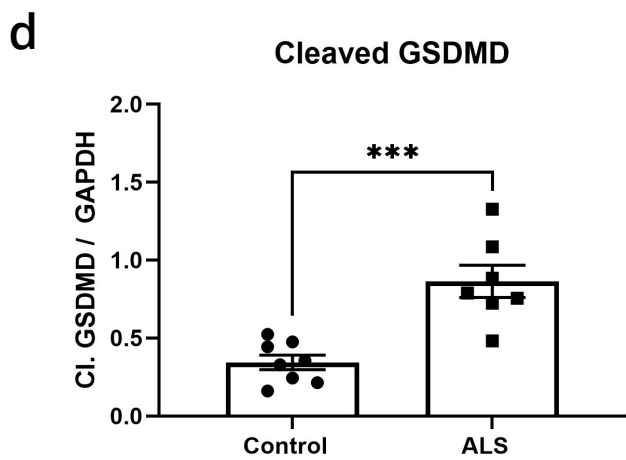# Figure 6. Biochemical characterization of pyroptosis proteins in the ALS spinal cord.
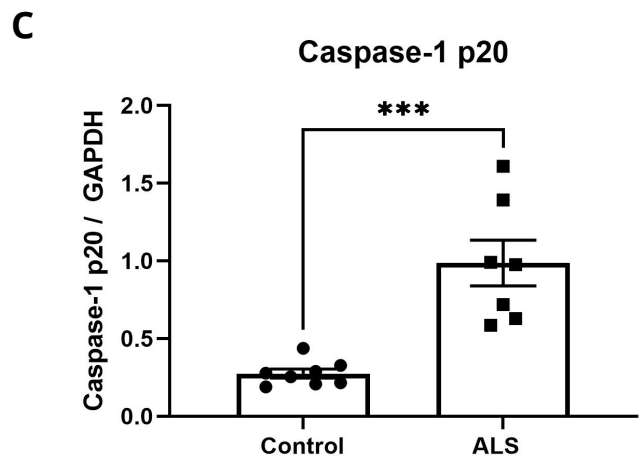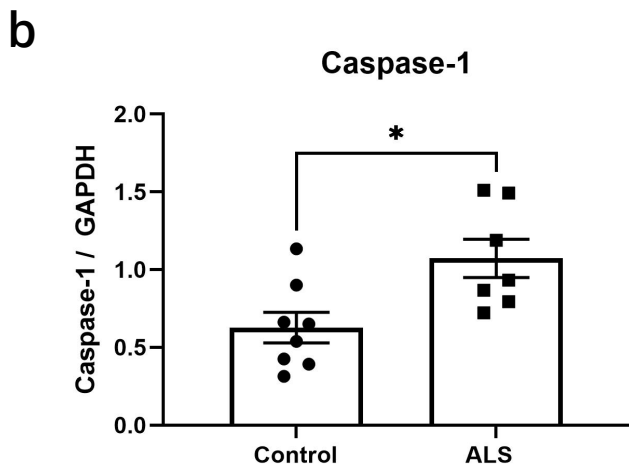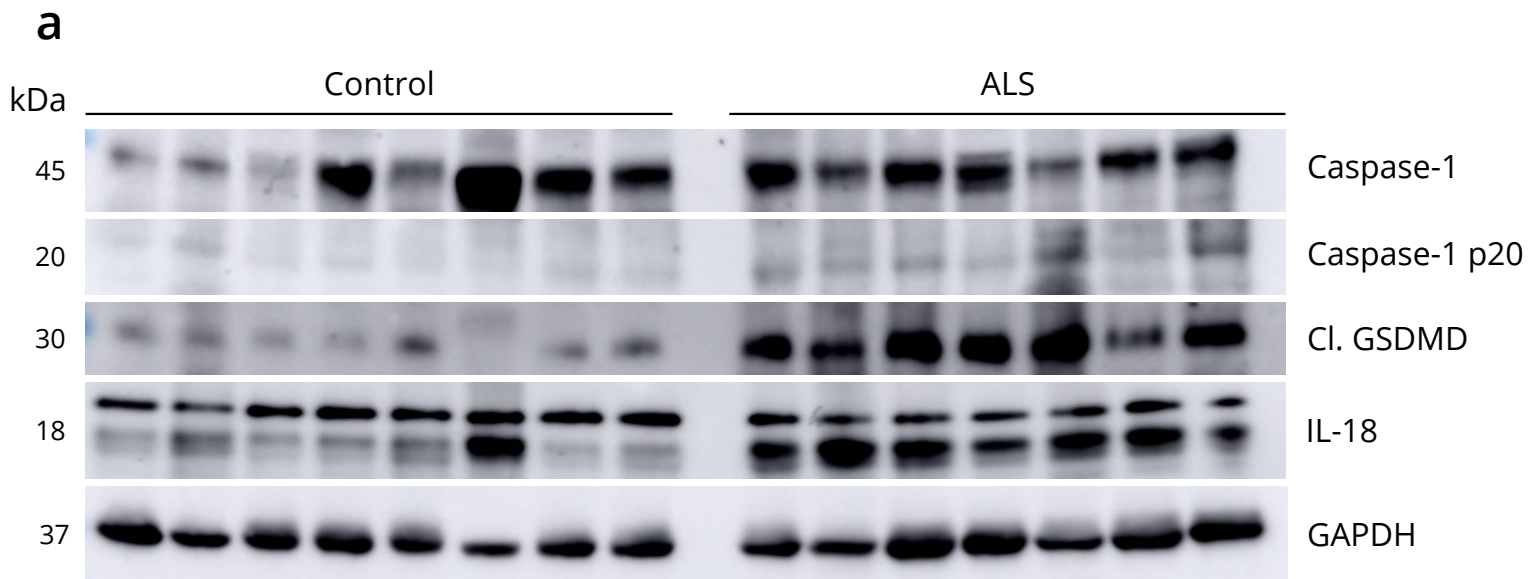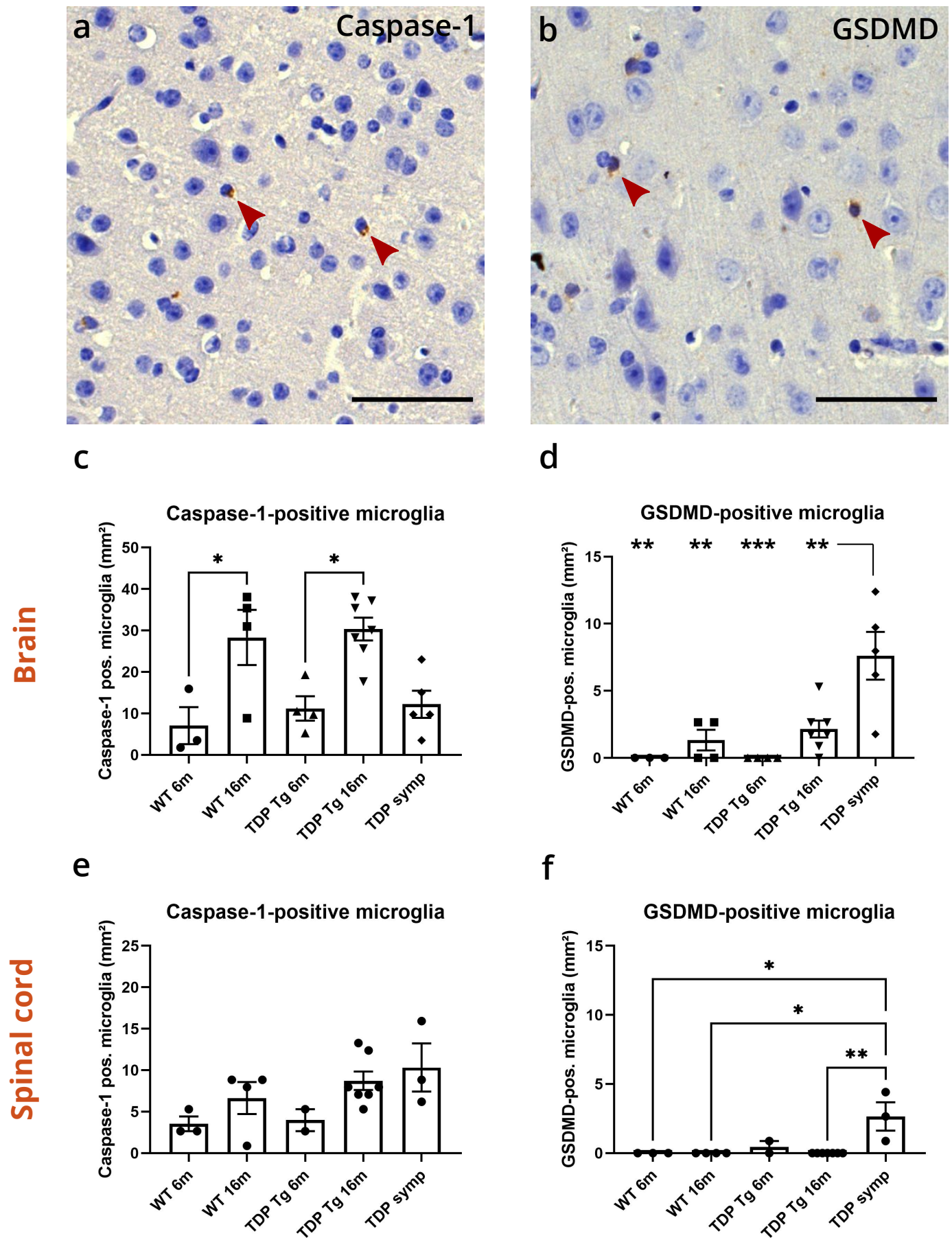
Figure 7. Increased expression of GSDMD in motor cortex and spinal cord of symptomatic TDP-43 A315T transgenic mice.

Supplementary material to:

Increased pyroptosis activation in white matter microglia is associated with neuronal loss in ALS motor cortex

Evelien Van Schoor (1,2,3), Simona Ospitalieri (1), Sebastiaan Moonen (1, 3, 4), Sandra O. Tomé (1), Alicja Ronisz (1), Orkun Ok (1), Jochen Weishaupt (5,6), Albert C. Ludolph (5,7), Philip Van Damme (2,3,8), Ludo Van Den Bosch (2,3), Dietmar Rudolf Thal (1,9)

Affiliations

1. Laboratory of Neuropathology, Department of Imaging and Pathology, KU Leuven (University of Leuven), Leuven Brain Institute (LBI), Leuven, Belgium.

2. Laboratory of Neurobiology, Department of Neurosciences, KU Leuven (University of Leuven), Leuven Brain Institute (LBI), Leuven, Belgium.

3. Center for Brain & Disease Research, VIB, Leuven, Belgium.

4. Laboratory for the Research of Neurodegenerative Diseases, Department of Neurosciences, KU Leuven (University of Leuven), Leuven Brain Institute (LBI), Leuven, Belgium

5. Department of Neurology, Ulm University, Ulm, Germany.

6. Divisions of Neurodegeneration, Department of Neurology, Mannheim Center for Translational Neurosciences, Medical Faculty Mannheim, Heidelberg University, Mannheim, Germany.

7. Deutsches Zentrum für Neurodegenerative Erkrankungen, Ulm, Germany.

8. Department of Neurology, University Hospitals Leuven, Leuven, Belgium.

9. Department of Pathology, University Hospitals Leuven, Leuven, Belgium.

Supplementary figures and tables

Suppl. Figure 1. Expression of inflammasome components and pyroptosis effector proteins in control precentral white matter microglia. Immunohistochemical detection of inflammasome components NLRP3 **(a)**, ASC **(b)** and caspase-1 **(c)**, as well as pyroptosis effector-related proteins cleaved GSDMD **(d)** and IL-18 **(e)** in control precentral white matter. Arrowheads indicate microglial cells positive for respective markers. Control cases positive for the respective markers were selected. Scale bars represent 25 µm.
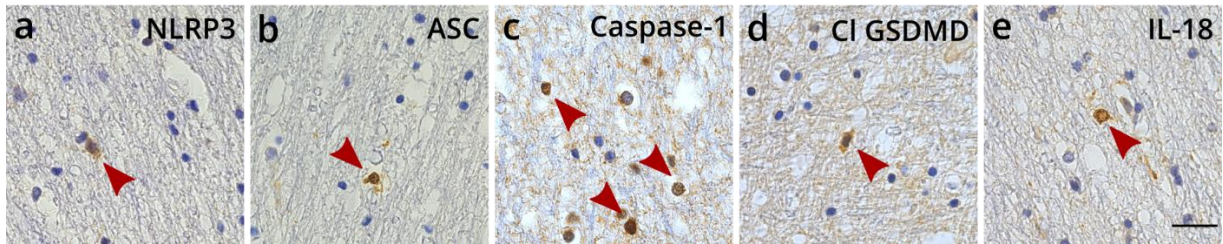
Suppl. Figure 2. Expression of cleaved GSDMD in ALS motor cortex in relation to astrocytes and oligodendrocytes. (a-h) Immunofluorescence detection of pyroptosis effector protein cleaved GSDMD in relation to GFAP-positive astrocytes (a-d) and Olig2-positive oligodendrocytes (e-h). Arrowheads indicate glial cells positive for cleaved GSDMD not overlapping with GFAP-positive astrocytes and Olig2-positive oligodendrocytes. Scale bars represent 50 µm.
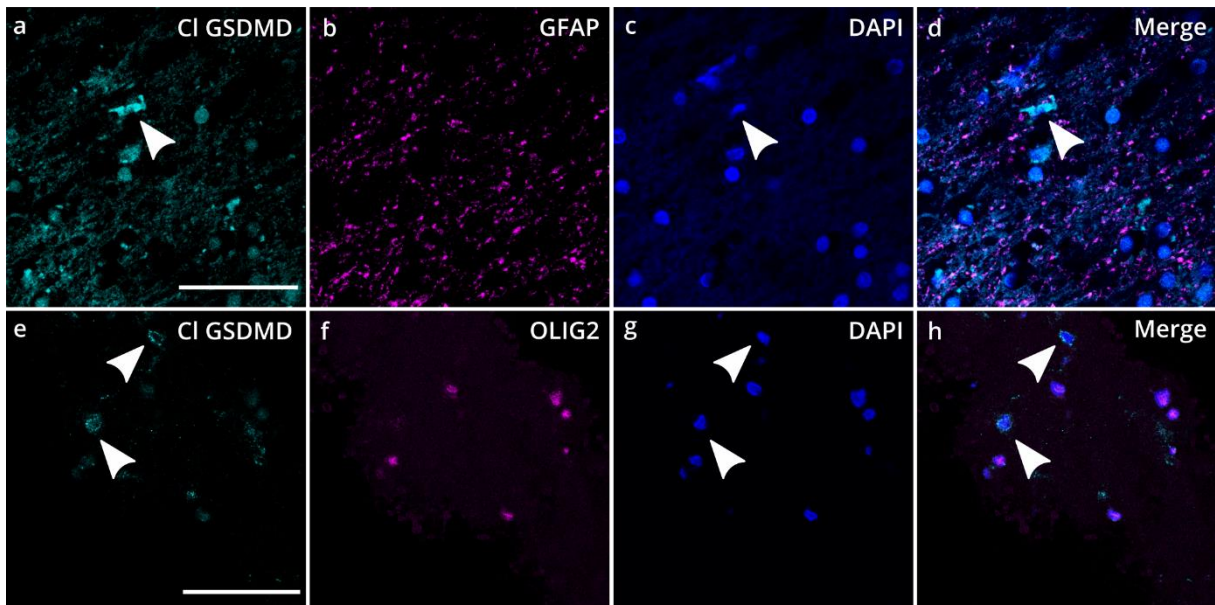
Suppl. Figure 3. Cleaved GSDMD expression in neurons in the ALS and control motor cortex. Graph representing the number of neurons in layer V of the motor cortex positive for cleaved GSDMD for control and ALS cases. Binary logistic regression corrected for age and sex was used for statistical analysis.
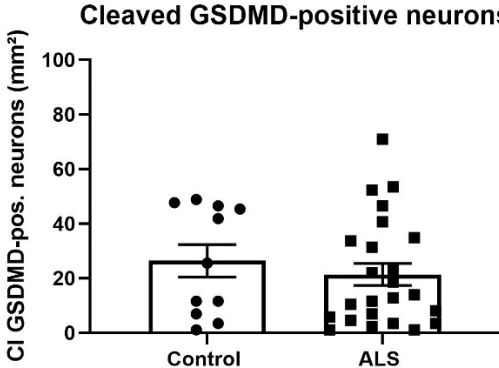
Suppl. Figure 4. Full western blots for the expression of pyroptosis proteins in the ALS motor cortex. (a-c) Full western blots for motor cortex tissue lysates from control (n = 7) and ALS (n = 8) probed with antibodies for caspase-1 (a), cleaved GSDMD (b) and IL-18 (c). Arrows indicate the bands at the correct molecular weight of the proteins. The case n° for each lane is indicated in a.
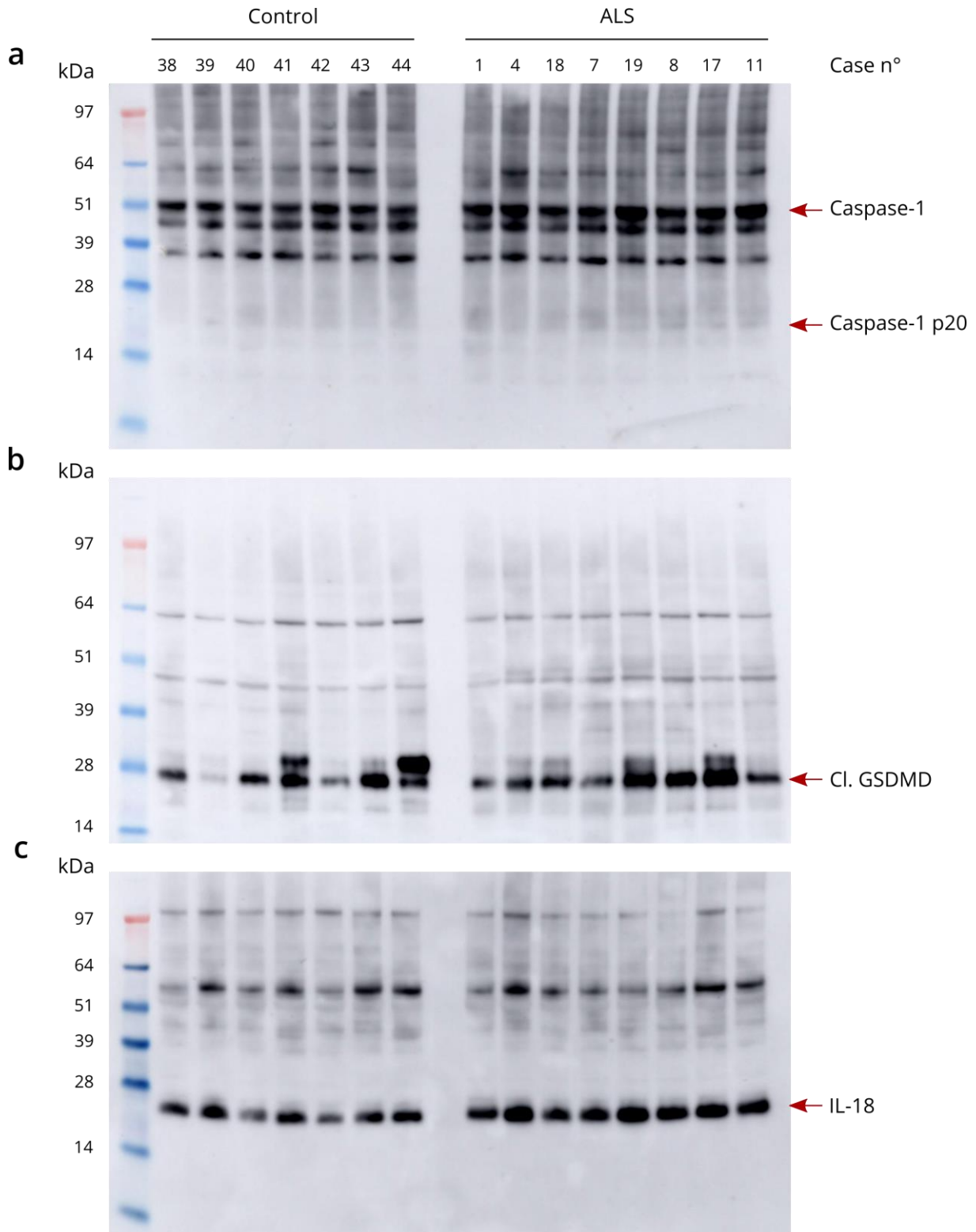
Suppl. Figure 5. Spinal cord anterior horn neuronal density and pTDP-43 pathology. (a) Graph representing the neuronal density per mm² in the anterior horn of the spinal cord of control and ALS cases. **(b)** Graph representing the percentage of pTDP-43 affected neurons in the spinal cord of control and ALS cases. Binary logistic regression corrected for age and sex (a) and Mann-Whitney U test (b) were used for statistical analysis. * $p < 0.05$; **** $p < 0.0001$.
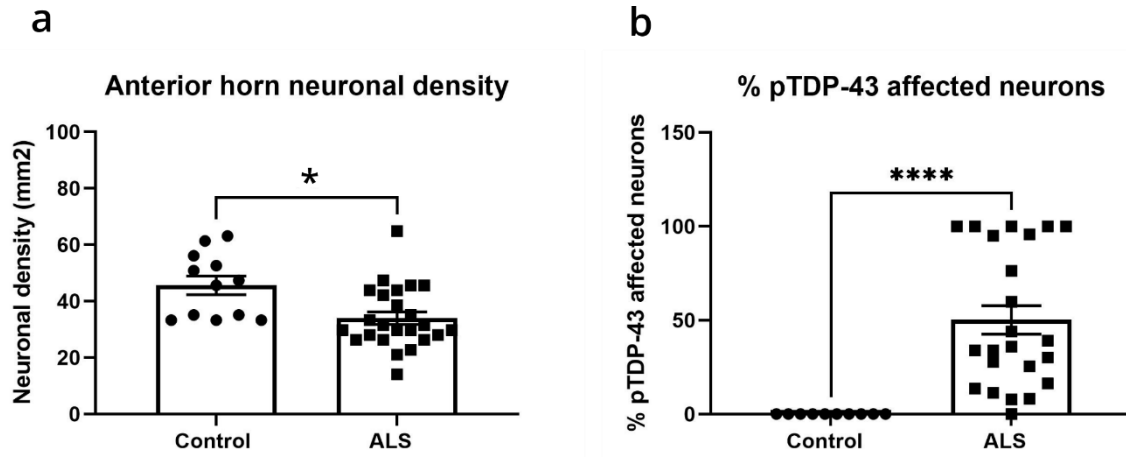
Suppl. Figure 6. Full western blots for the expression of pyroptosis proteins in the ALS spinal cord. (a-c) Full western blots for spinal cord tissue lysates from control (n = 8) and ALS (n = 7) probed with antibodies for caspase-1 (a), cleaved GSDMD (b) and IL-18 (c). Arrows indicate the bands at the correct molecular weight of the proteins. The extra lane for IL-18 (c) is a positive control (+). The case n° for each lane is indicated in a.
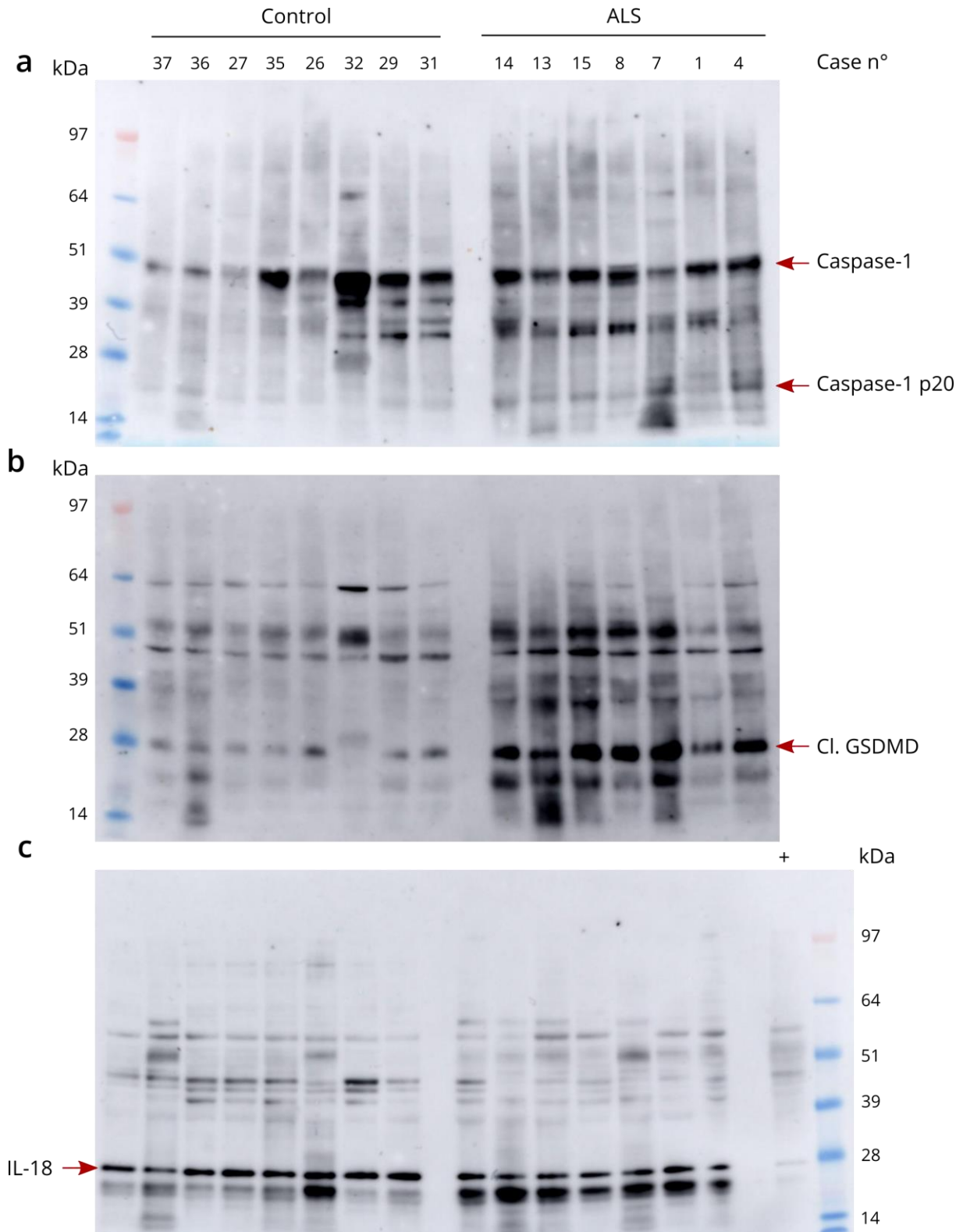
Suppl. Figure 7. Caspase-1 and GSDMD are expressed in microglia in TDP-43^{A315T} transgenic mice. Immunofluorescence detection of caspase-1 **(a-d)** and GSDMD **(e-h)** in Iba-1-positive microglia in the CNS of symptomatic TDP-43^{A315T} transgenic mice. Merge of all three channels is shown. Arrowheads indicate microglia positive for caspase-1 (a-d) and GSDMD (e-h). Scale bars represent 25 µm.
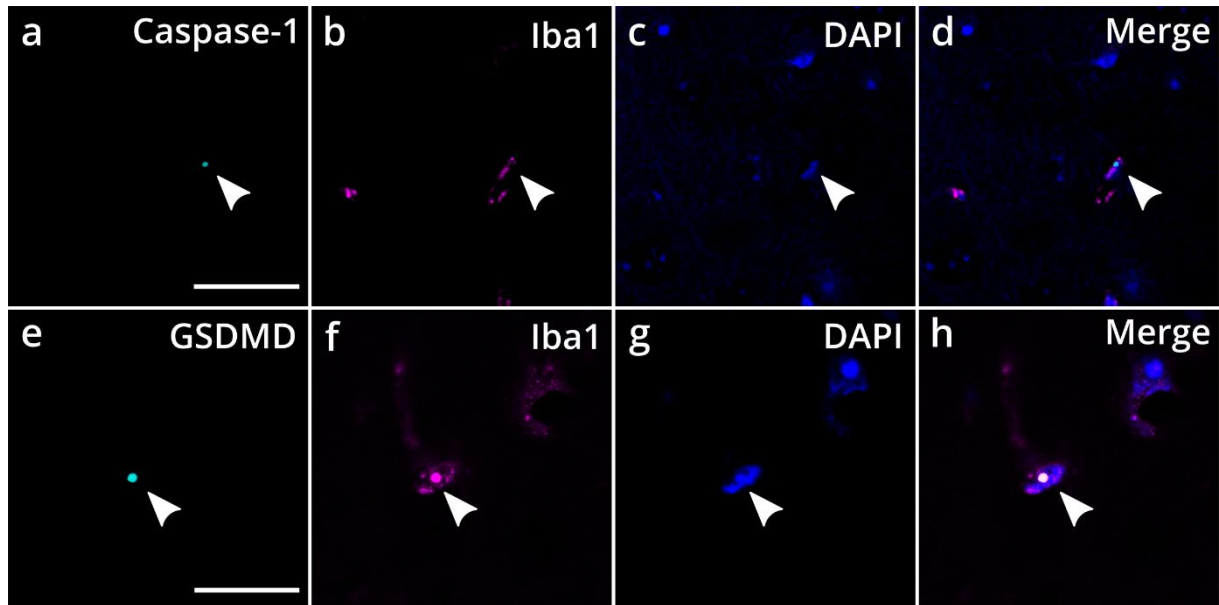
Suppl. Figure 8. Increased TDP-43 nuclear clearance in the motor cortex and spinal cord of symptomatic TDP-43^{A315T} transgenic mice. (a, b) Immunohistochemical representative images of an antibody staining against TDP-43 in the brain (a) and spinal cord (b) of symptomatic TDP-43^{A315T} transgenic mice. Arrowheads indicate neuronal nuclei cleared of TDP-43. Arrow indicates perinuclear dens aggregated TDP-43-positive material with the nucleus devoid of TDP-43. Scale bars represent 50 µm. **(c, d)** Graphs representing the percentage of neurons cleared of nuclear TDP-43 in the brain (c) and spinal cord (d) for the different groups of mice. WT 6m = 6 months old wild-type mice; WT 16m = 16 months old wild-type mice; TDP Tg 6m = 6 months old TDP-43^{A315T} transgenic mice; TDP Tg 16m = 16 months old TDP-43^{A315T} transgenic mice; TDP symp = symptomatic TDP^{A315T} transgenic mice. ** $p < 0.01$.
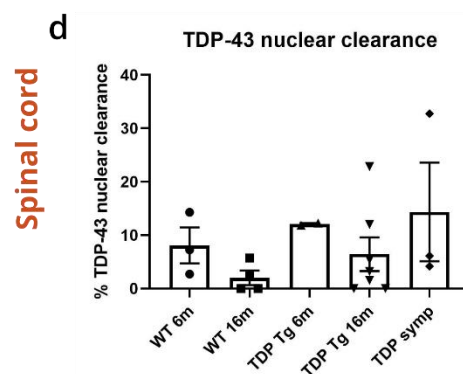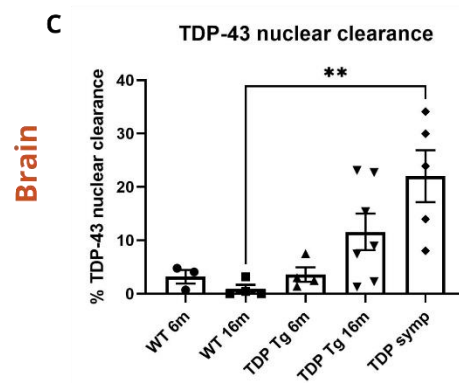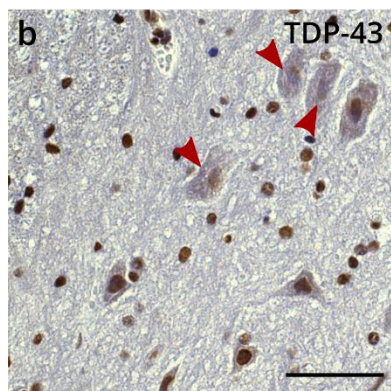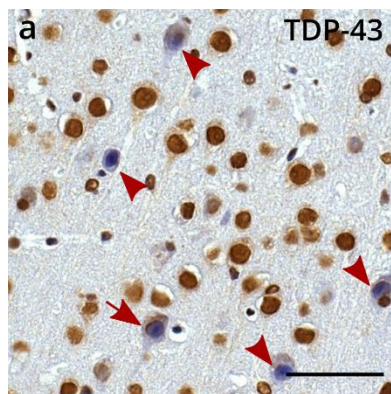
Suppl. Figure 9. Ubiquitin and SQSTM1/p62 pathology in the motor cortex and spinal cord of TDP-43^{A315T} transgenic mice. (a, b) Immunohistochemical representative images of ubiquitin-positive cytoplasmic staining in motor neurons in the motor cortex (a) and in the anterior horn of the spinal cord (b) of symptomatic TDP-43^{A315T} transgenic mice. Arrowheads indicate neurons positive for ubiquitin. **(c, d)** Immunohistochemical representative images of SQSTM1/p62-positive cytoplasmic staining in motor neurons in the motor cortex (c) and in the anterior horn of the spinal cord (d) of symptomatic TDP-43^{A315T} transgenic mice. Arrowheads indicate neurons positive for SQSTM1/p62. Scale bars represent 25 µm (a,b) and 50 µm (c,d).
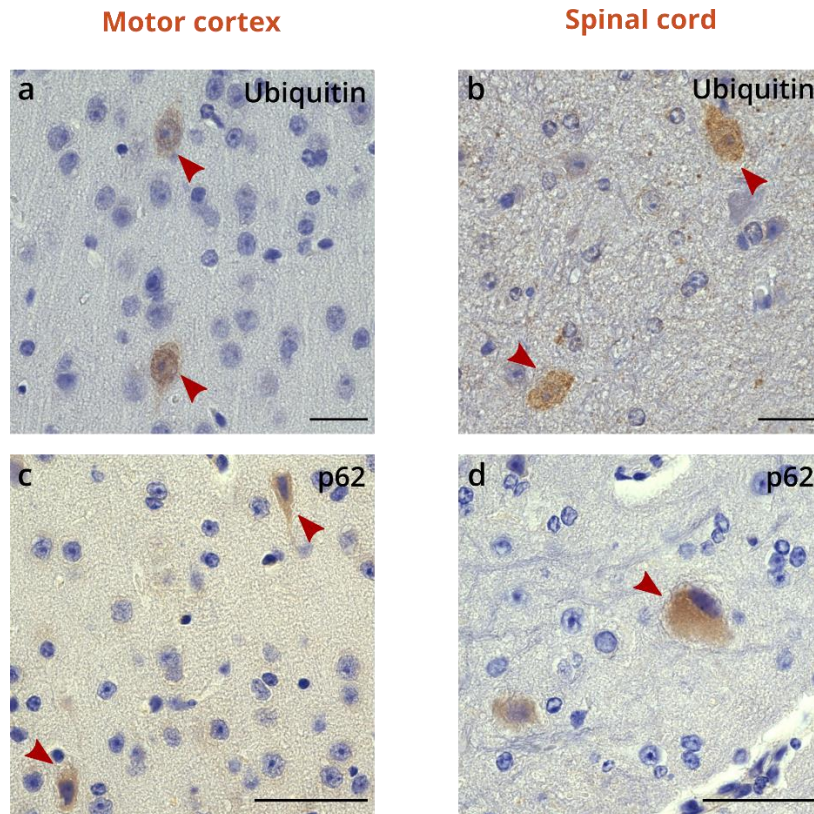
Suppl. Figure 10. Neuronal density in the motor cortex and spinal cord of TDP-43^{A315} transgenic mice. Graphs representing the neuronal density per mm² for layer V of the motor cortex in the brain **(a)** and for the anterior horn of the spinal cord **(b)** for the different groups of mice. WT 6m = 6 months old wild-type mice; WT 16m = 16 months old wild-type mice; TDP Tg 6m = 6 months old TDP-43^{A315T} transgenic mice; TDP Tg 16m = 16 months old TDP-43^{A315T} transgenic mice; TDP symp = symptomatic TDP^{A315T} transgenic mice. * $p < 0.05$.
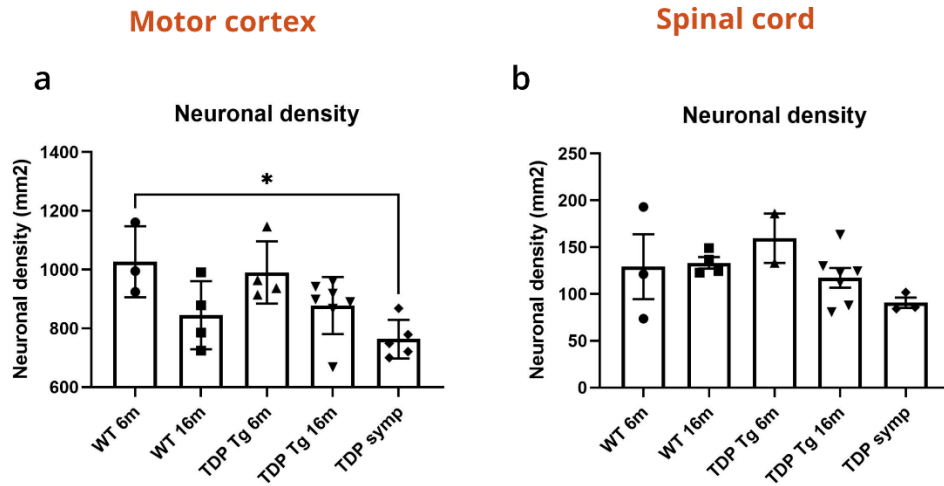
Suppl. Table 1. List of human cases. The table provides information regarding age (= age at death), sex, diagnosis, the presence of the *C9orf72* mutation, AβMTL phase, Braak NFT stage, CERAD score, disease duration (months), PMI (hours) and application (western blot / immunohistochemistry). Abbreviations: f = female; m = male; ALS = amyotrophic lateral sclerosis; FTLD = frontotemporal lobar degeneration; control = non neurodegenerative disease control; A = aneurysm; AGD = argyrophilic grain disease; ARTAG = aging-related tau astrogliopathy; CM = carcinoma metastasis; GB = Guillian-Barre syndrome; I = infarction; MI = microinfarction; n.a. = not applicable; n.d. = not determined; PART = primary age-related tauopathy; p-preAD = preclinical preAD; SVD = small vessel disease; SVE = subcortical vascular encephalopathy; PMI = *post-mortem* interval; WB = western blot; IHC = immunohistochemistry.

Case n°	Age	Sex	Diagnosis	C9 mutation	AβMTL phase	Braak NFT stage	CERAD	Disease duration	PMI (hours)	Application
1	58	f	ALS, PART	0	0	2	0	18 months	24	WB, IHC
2	62	f	ALS	0	0	1	0	12 months	24	IHC
3	51	m	ALS	0	0	1	0	8 months	24	IHC
4	49	m	ALS, PART	0	0	1	0	45 months	24	WB, IHC
5	46	m	ALS	0	0	1	0	40 months	24	IHC
6	62	m	ALS, MI, I, ARTAG, PART, AGD	0	0	1	0	154 months	12	IHC
7	53	m	ALS	0	0	1	0	92 months	24	WB, IHC
8	74	m	ALS	0	1	1	0	47 months	24	WB, IHC
9	68	f	ALS	0	0	1	0	n.d.	192	IHC
10	56	f	ALS	0	1	1	0	48 months	72	IHC
11	57	f	ALS, FTLD-TDP Type B	0	1	1	0	22 months	24	WB, IHC
12	61	m	ALS, FTLD-TDP Type B	0	0	1	0	32 months	2	IHC
13	50	f	ALS	0	0	1	0	18 months	24	WB, IHC
14	54	m	ALS	0	0	1	0	88 months	6	WB, IHC
15	69	f	ALS	0	1	1	0	6 months	24	WB
16	68	m	ALS, SVD	1	2	1	0	n.d.	144	IHC
17	52	m	ALS	1	0	0	0	15 months	6	WB, IHC
18	57	m	ALS, p-preAD	1	1	1	0	17 months	n.d.	WB, IHC
19	49	m	ALS, PART	1	0	1	0	46 months	24	WB, IHC
20	48	m	ALS	1	0	1	0	18 months	24	IHC
21	57	m	ALS	1	0	1	0	19 months	20	IHC
22	75	m	ALS	1	0	2	0	n.d.	24	IHC
23	50	m	ALS, Wernicke encephalopathy	1	0	1	0	n.d.	24	IHC
24	46	f	ALS	1	0	1	0	20 months	120	IHC
25	55	m	ALS, FTLD-TDP Type B	1	0	3	0	30 months	12	IHC
26	45	m	Control, I	n.d.	0	0	0	n.a.	24	WB, IHC
27	46	m	Control	n.d.	0	1	0	n.a.	29	WB, IHC
28	74	m	Control, CM, I, MI	n.d.	0	0	0	n.a.	72	IHC
29	61	m	Control, SVD	n.d.	0	0	0	n.a.	48	WB, IHC
30	73	m	Control, SVD, CM	n.d.	0	2	0	n.a.	48	IHC
31	55	m	Control, A, I	n.d.	0	0	0	n.a.	96	WB, IHC
32	74	f	Control, AGD, SVE	n.d.	0	1	0	n.a.	24	WB, IHC
33	35	m	Control, Limbic encephalitis	n.d.	0	0	0	n.a.	72	IHC
34	54	m	Control, GB	n.d.	0	1	0	n.a.	24	IHC
35	63	f	Control, MI	n.d.	0	1	0	n.a.	96	WB, IHC
36	64	m	Control	n.d.	0	0	0	n.a.	96	WB, IHC
37	35	m	Control	n.d.	0	1	0	n.a.	48	WB, IHC
38	64	f	Control, MI	n.d.	1	1	0	n.a.	48	WB
39	66	m	Control	n.d.	2	2	0	n.a.	6	WB
40	68	f	Control, I, MI, SVD	n.d.	3	1	0	n.a.	24	WB
41	68	m	Control	n.d.	3	1	0	n.a.	48	WB
42	64	f	Control, I	n.d.	0	1	0	n.a.	n.d.	WB
43	67	f	Control, ARTAG	n.d.	3	2	0	n.a.	n.d.	WB
44	59	m	Control, I	n.d.	2	1	0	n.a.	72	WB

Suppl. Table 2. List of antibodies used in the study. The table summarizes information about host, clonality, supplier and catalog number of the primary antibodies used for immunohistochemistry (IHC), immunofluorescence (IF) and western blot (WB). Dilutions for IHC (human and mouse tissue), IF (human and mouse tissue) and WB (human tissue) are given.

Primary antibody	Host	Clonality	Supplier	Catalog number	Human IHC	Mouse IHC	Mouse IF	Human IF	Human WB
Cleaved GSDMD (Asp275)	Rabbit	Monoclonal	Cell Signaling	36425	1:400	-	-	1:200	-
GSDMD-NT	Rabbit	Polyclonal	Protein Tech	20770-1-AP	-	-	-	-	1:5000
Gasdermin D	Rabbit	Monoclonal	Abcam	ab219800	-	1:100	1:50	-	-
Caspase-1	Mouse	Monoclonal	Adipogen	AG-20B-0048-C100	1:100	-	-	1:50	1:1000
Caspase-1	Rabbit	Polyclonal	Abcam	ab138483	-	1:400	1:300	-	-
IL-18	Rabbit	Polyclonal	Protein Tech	10663-1-AP	1:50	-	-	1:50	1:1000
ASC	Mouse	Monoclonal	Santa Cruz	sc-514414	1:250	-	-	1:50	-
NLRP3	Rabbit	Polyclonal	ABIN	ABIN1386361	1:200	-	-	1:50	-
pTDP43 (S409/410-2)	Rabbit	Polyclonal	Cosmo Bio	TIP-PTD-P02	1:5000	-	-	-	-
pTDP43 (S409/410-1)	Mouse	Monoclonal	Cosmo Bio	TIP-PTD-M01	1:5000	-	-	-	-
TDP-43	Rabbit	Polyclonal	Protein Tech	12892-1-AP	1:1000	1:1000	-	-	-
Ubiquitin	Rabbit	Polyclonal	Protein Tech	10201-2-AP	-	1:10 000	-	-	-
Iba1	Goat	Polyclonal	Abcam	ab5076	-	-	1:200	1:200	-
GFAP	Guinea Pig	Polyclonal	Synaptic Systems	173 004	-	-	-	1:300	-
Olig2	Rabbit	Monoclonal	Abcam	ab109186	-	-	-	1:100	-
β-Amyloid (clone 4G8)	Mouse	Monoclonal	BioLegend	SIG-39220	1:5000	-	-	-	-
pTau (S202/T205) (clone AT8)	Mouse	Monoclonal	ThermoFisher	MN1020	1:1000	-	-	-	-
GAPDH (clone 6C5)	Mouse	Monoclonal	ThermoFisher	AM4300	-	-	-	-	1:10 000
SQSTM1/p62	Mouse	Monoclonal	BD Transduction	610832	-	1:250	-	-	-

Suppl. Table 3. Detailed information on binary logistic regression analyses.

(1) Binary logistic regression addressing the differences between control and ALS cases regarding caspase-1-positive microglia in layer V of the motor cortex, when controlled for age and sex.

	Sign.	Odds ratio	95% CI OR: lower	95% CI OR: upper
Caspase-1-pos. microglia motor cortex layer V	**p = 0.031***	0.975	0.954	0.998
Age at death	p = 0.727	0.986	0.912	1.066
Sex	p = 0.504	0.511	0.072	3.656

(2) Binary logistic regression addressing the differences between control and ALS cases regarding cleaved GSDMD-positive microglia in layer V of the motor cortex, when controlled for age and sex.

	Sign.	Odds ratio	95% CI OR: lower	95% CI OR: upper
Cl. GSDMD-pos. microglia motor cortex layer V	p = 0.345	1.138	0.870	1.488
Age at death	p = 0.343	0.961	0.886	1.043
Sex	p = 0.235	0.286	0.036	2.251

(3) Binary logistic regression addressing the differences between control and ALS cases regarding cleaved GSDMD-positive neurons in layer V of the motor cortex, when controlled for age and sex.

	Sign.	Odds ratio	95% CI OR: lower	95% CI OR: upper
Cl. GSDMD-pos. neurons motor cortex layer V	p = 0.527	0.988	0.952	1.025
Age at death	p = 0.805	0.991	0.921	1.066
Sex	p = 0.491	0.533	0.089	3.193

(4) Binary logistic regression addressing the differences between control and ALS cases regarding caspase-1-positive microglia in the precentral white matter, when controlled for age and sex.

	Sign.	Odds ratio	95% CI OR: lower	95% CI OR: upper
Caspase-1-pos. microglia precentral white matter	p = 0.400	1.006	0.992	1.020
Age at death	p = 0.711	0.987	0.919	1.060
Sex	p = 0.476	0.506	0.078	3.300

(5) Binary logistic regression addressing the differences between control and ALS cases regarding cleaved GSDMD-positive microglia in the precentral white matter, when controlled for age and sex.

	Sign.	Odds ratio	95% CI OR: lower	95% CI OR: upper
Cl. GSDMD-pos. microglia precentral white matter	**p = 0.034***	1.155	1.011	1.319
Age at death	p = 0.596	0.976	0.890	1.069
Sex	p = 0.089	0.143	0.015	1.349

(6) Binary logistic regression addressing the differences between control and ALS cases regarding motor cortex layer V neuronal density, when controlled for age and sex.

	Sign.	Odds ratio	95% CI OR: lower	95% CI OR: upper
Motor cortex layer V neuronal density	**p = 0.023***	0.880	0.788	0.982
Age at death	p = 0.486	0.953	0.832	1.091
Sex	p = 0.710	2.002	0.052	77.547

(7) Binary logistic regression addressing the differences between control and ALS cases regarding the percentage of neurons with TDP-43 cleared from the nucleus in layer V of the motor cortex, when controlled for age and sex.

	Sign.	Odds ratio	95% CI OR: lower	95% CI OR: upper
% of neurons with TDP-43 nuclear clearance	**p = 0.022***	1.179	1.023	1.358
Age at death	p = 0.587	1.027	0.932	1.133
Sex	p = 0.517	2.488	0.158	39.212

(8) Binary logistic regression addressing the differences between control and ALS cases regarding caspase-1-positive microglia in the ventral pyramidal tracts, when controlled for age and sex.

	Sign.	Odds ratio	95% CI OR: lower	95% CI OR: upper
Caspase-1-pos. microglia ventral pyr. tracts	p = 0.270	0.947	0.860	1.043
Age at death	p = 0.960	0.998	0.924	1.078
Sex	p = 0.450	0.467	0.065	3.370

(9) Binary logistic regression addressing the differences between control and ALS cases regarding caspase-1-positive microglia in the lateral pyramidal tracts, when controlled for age and sex.

	Sign.	Odds ratio	95% CI OR: lower	95% CI OR: upper
Caspase-1-pos. microglia lateral pyr. tracts	p = 0.606	1.002	0.994	1.010
Age at death	p = 0.865	1.007	0.932	1.087
Sex	p = 0.680	0.668	0.098	4.538

(10) Binary logistic regression addressing the differences between control and ALS cases regarding cleaved GSDMD-positive microglia in the ventral pyramidal tracts, when controlled for age and sex.

	Sign.	Odds ratio	95% CI OR: lower	95% CI OR: upper
Cl. GSDMD-pos. microglia ventral pyr. tracts	p = 0.216	1.285	0.864	1.912
Age at death	p = 0.875	1.006	0.934	1.084
Sex	p = 0.522	0.541	0.083	3.542

(11) Binary logistic regression addressing the differences between control and ALS cases regarding cleaved GSDMD-positive microglia in the lateral pyramidal tracts, when controlled for age and sex.

	Sign.	Odds ratio	95% CI OR: lower	95% CI OR: upper
Cl. GSDMD-pos. microglia lateral pyr. tracts	p = 0.172	1.086	0.965	1.224
Age at death	p = 0.862	1.007	0.934	1.085
Sex	p = 0.500	0.508	0.071	3.624

(12) Binary logistic regression addressing the differences between control and ALS cases regarding the anterior horn neuronal density, when controlled for age and sex.

	Sign.	Odds ratio	95% CI OR: lower	95% CI OR: upper
Anterior horn neuronal density	**p = 0.017***	0.912	0.846	0.984
Age at death	p = 0.627	0.982	0.911	1.058
Sex	p = 0.725	0.703	0.099	4.991

Suppl. Table 4. Linear regression model for motor cortex neuronal density. Influence of predictor variables, i.e. the number of cleaved GSDMD-positive microglia in the precentral white matter, the number of caspase-1-positive microglia in the precentral white matter, and the percentage of pTDP-43 affected neurons in the motor cortex on motor cortex layer V neuronal density in different linear regression model terms as defined in parts 1 and 2. Age and sex were included in the model as potential confounders but were not statistically significant. $* p < 0.05$; $** p < 0.01$.

Part 1

Predictor variable	Coefficient β	*p* value
% pTDP-43 affected neurons	-0.435	p = 0.010*
Age	-0.252	p = 0.124
Gender	-0.003	p = 0.983

Dependent variable: Motor cortex layer V neuronal density

Predictor variable	Coefficient β	*p* value
Cl GSDMD-positive microglia	-0.455	p = 0.021*
Age	-0.190	p = 0.315
Sex	0.195	p = 0.308

Dependent variable: Motor cortex layer V neuronal density

Predictor variable	Coefficient β	*p* value
Caspase-1-positive microglia	-0.244	p = 0.179
Age	-0.220	p = 0.217
Sex	0.035	p = 0.846

Dependent variable: Motor cortex layer V neuronal density

Part 2

Predictor variable	Coefficient β	*p* value
Cl GSDMD-positive microglia	-0.464	p = 0.007**
% pTDP-43 affected neurons	-0.486	p = 0.004**
Age	-0.248	p = 0.134
Sex	0.157	p = 0.340

Dependent variable: Motor cortex layer V neuronal density

Suppl. Table 5. Correlation matrix for spinal cord neuronal density and other parameters, corrected for age and sex. Matrix showing Pearson's correlation values and p-values for the association between spinal cord anterior horn neuronal density and other variables, including the number of caspase-1-positive microglia in the spinal cord lateral white matter tracts, the number of cleaved GSDMD-positive microglia in the spinal cord lateral white matter tracts, and the percentage of pTDP-43 affected neurons in the spinal cord. ** $p < 0.01$.

	Caspase-1-positive microglia	Cleaved GSDMD-positive microglia	% pTDP-43 affected neurons	Neuronal density	n
Caspase-1 positive microglia	-				23
Cleaved GSDMD-positive microglia	r = -0.119; p = 0.571	-			23
% pTDP-43 affected neurons	r = -0.162; p = 0.439	r = 0.208; p = 0.318	-		23
Neuronal density anterior horn	r = -0.200; p = 0.337	r = 0.045; p = 0.832	r = -0.554; p = 0.004**	-	23

Suppl. Table 6. Correlation matrix for mouse spinal cord neuronal density and other parameters. Matrix showing Pearson's correlation values and p-values for the association between mouse spinal cord neuronal density and other variables, including the number of caspase-1-positive microglia, the number of GSDMD-positive microglia, and the percentage of TDP-43 nuclear clearance.

	Caspase-1-positive microglia	GSDMD-positive microglia	% TDP clearance	Neuronal density	n
Caspase-1-positive microglia	-				19
GSDMD-positive microglia	r = 0.201; p = 0.410	-			19
% TDP clearance	r = -0.144; p = 0.556	r = 0.058; p = 0.815	-		19
Neuronal density	r = -0.146; p = 0.556	r = -0.392; p = 0.097	r = -0.174; p = 0.476	-	19